Homology-directed repair using next-generation CRISPR/Cpf1-geminiviral replicons in tomato

Tien Van Vu[1,2], Velu Sivankalyani[1], Eun-Jung Kim[1], Mil Thi Tran[1], Jihae Kim[1], Yeon Woo Sung[1], Duong Thi Hai Doan[1], Minwoo Park[3], Jae-Yean Kim[1,4,*]

[1]Division of Applied Life Science (BK21 Plus program), Plant Molecular Biology and Biotechnology Research Center, Gyeongsang National University, Jinju 660-701, Republic of Korea.

[2]National Key Laboratory for Plant Cell Biotechnology, Agricultural Genetics Institute, Km 02, Pham Van Dong road, Co Nhue 1, Bac Tu Liem, Hanoi 11917, Vietnam.

[3]Hyundai Seed Co., LTD., 286, Yeonsam-ro, Ganam, Yeoju, Gyeonggi-do, 12660, Korea.

[4]Division of Life Science, Gyeongsang National University, 501 Jinju-daero, Jinju 52828, Republic of Korea.

*** Correspondence: Jae-Yean Kim (kimjy@gnu.ac.kr)**

ABSTRACT

Genome editing via the homology-directed repair (HDR) pathway in somatic plant cells is very inefficient compared to error-prone repair by nonhomologous end joining (NHEJ). Here, we increased HDR-based genome editing efficiency approximately 3-fold compared to a Cas9-based single-replicon system via the use of *de novo* multiple replicon systems equipped with CRISPR/LbCpf1 in tomato and obtained replicon-free but stable HDR alleles. The efficiency of CRISPR/LbCpf1-based HDR was significantly modulated by physical culture conditions such as temperature and light. Ten days of incubation at 31°C under a light/dark cycle after *Agrobacterium*-mediated transformation resulted in

the best performance among the tested conditions. Furthermore, we developed our single-replicon system into a next-generation multiple replicon system that effectively increased HDR efficiency. Although this approach is still challenging, we showed the feasibility of HDR-based genome editing of a salt-tolerant SlHKT1;2 allele without genomic integration of antibiotic markers or any phenotypic selection. Self-pollinated offspring plants carrying the HKT1;2 HDR allele showed stable inheritance and germination tolerance in the presence of 100 mM NaCl. Our work may pave the way for transgene-free editing of alleles of interest in asexually as well as sexually reproducing plants.

Key words: homology-directed repair (HDR), gene targeting, CRISPR/Cpf1, allele replacement, Multiple replicon.

Running title: Advancement of plant HDR by multiple replicons.

INTRODUCTION

In plant somatic cells, double-strand DNA breaks (DSBs) are efficiently repaired by a nonhomologous end joining (NHEJ) mechanism, which dominates over the homology-directed repair (HDR) pathway (Jiang et al., 2013; Puchta, 2005). NHEJ repair usually leads to various types of mutations including DNA sequence insertions, deletions (Hsu et al., 2014; Zetsche et al., 2015), chromosome rearrangement, or chromosome relocation (Ferguson and Alt, 2001; Richardson et al., 1998; Varga and Aplan, 2005). Early in the 1990s, a transgenic approach using yeast mitochondrial I-Sce I endonuclease as a DSB inducer was adopted in attempts to investigate the mechanisms of DSB repair in plants, especially gene targeting via the HDR pathway in plant somatic cells (Fauser et al., 2012; Puchta et al., 1993), which have been the

main targets of recent plant genome engineering approaches (Baltes et al., 2014; Belhaj et al., 2013; Cermak et al., 2015; Nekrasov et al., 2013). In plant somatic cells, the HDR pathway employs homologous DNA templates to precisely repair damaged DNA, mainly via the synthesis-dependent strand annealing (SDSA) mechanism, with an extremely low efficiency(Puchta et al., 1996; Szostak et al., 1983), leading to difficulties in practical applications. Therefore, research on plant gene targeting has continued to focus on improving HDR efficacy. Previously reported data have indicated two most important factors affecting HDR efficiency in plant somatic cells: DSB formation and the amount of homologous DNA templates available at sites of breakage (Baltes et al., 2014; Endo et al., 2016; Puchta, 2005; Puchta et al., 1993; Townsend et al., 2009).

The recent development of the clustered regularly interspaced short palindromic repeats (CRISPR)/CRISPR-associated protein (Cas) system has provided excellent molecular scissors the generation of DSBs. *Streptococcus pyogenes* Cas 9 (SpCas9) (Sapranauskas et al., 2011) and *Lachnospiraceae bacterium* Cas12a (LbCas12a or LbCpf1) (Zetsche et al., 2015) have been adapted for wide use in genome engineering studies in various kingdoms including Plantae (Barrangou and Doudna, 2016; Hsu et al., 2014; Jinek et al., 2012). The former system generally generates blunt ends (Jinek et al., 2012) at DSBs, while the latter cuts in a cohesive end configuration (Zetsche et al., 2015). As a consequence of DSB repair by NHEJ, the two types of CRISPR complexes exhibit comparably high indel mutation rates under *in vivo* conditions, thus proving to be ideal tools for DSB formation for initiating targeted HDR in plants. Furthermore, it has been suggested that the Cpf1 complex might present an advantage in HDR-based genome editing compared to the Cas9 complex because the cutting site of Cpf1 is located distal to the core target sequence and the protospacer-adjacent motif (PAM), allowing recutting even after

indel mutations are introduced during NHEJ-mediated repair (Baltes et al., 2014; Zetsche et al., 2015). CRISPR/Cpf1 complexes were recently successfully applied for gene targeting in plants(Li et al., 2018), providing alternative options for T-rich target site selection.

Because of the highly efficient replication of geminivirus genomes and their single-stranded DNA nature, these genomes have been used as perfect DNA template cargo for gene targeting in plants. Geminiviral genomic DNAs have been reconstructed to exogenously overexpress foreign proteins in plants at up to 80-fold higher levels compared to those of conventional T-DNA (Mor et al., 2003; Needham et al., 1998; Zhang and Mason, 2006) systems, due to their highly autonomous replication inside host nuclei and the ability to reprogram cells (Gutierrez, 1999; Hanley-Bowdoin et al., 2013). Furthermore, Rep/RepA has been reported to promote a cell environment that is permissive for homologous recombination to stimulate the replication of viral DNA. Interestingly, it has been reported that somatic homologous recombination is promoted by geminiviral infection (Richter et al., 2014). The above characteristics of geminiviral replicons have been shown to make them perfect delivery tools for introducing large amounts of homologous donor templates to plant nuclei. Likewise, the movement and coat proteins of a bean yellow dwarf virus (BeYDV)–based replicon were removed and replaced with Cas9 or TALEN to improve gene targeting in plants (Baltes et al., 2014; Butler et al., 2016; Cermak et al., 2015; Dahan-Meir et al., 2018; Gil-Humanes et al., 2017; Hummel et al., 2018). The LbCpf1 complex, which was subsequently discovered and adapted for plant genome editing in 2015, has not been tested in combination with geminiviral replicon systems for plant gene targeting.

Despite higher success rates in gene targeting in plants using the geminiviral replicon system, most of the reported cases have required markers associated with the edited alleles, while the selection and regeneration of HDR events from edited cells are still challenging (Butler et al.,

2016; Gil-Humanes et al., 2017; Hummel et al., 2018). In addition, the effective application of replicon cargos in plant gene targeting has been shown to be limited by their size (Baltes et al., 2014; Suarez-Lopez and Gutierrez, 1997). Therefore, plant gene targeting, especially in cases of marker-free alleles, still requires improvement. We hypothesized that the combination of the repeatedly cutting nature of a CRISPR/Cpf1 complex and the highly autonomous replication of *de novo*-engineered geminiviral replicon systems could overcome the efficacy barrier of marker-free gene targeting via the HDR pathway in plants. Here, we report significant improvement of homology-directed repair using next-generation CRISPR/LbCpf1-geminiviral replicons in tomato and the successful application of the system to target a marker-free salt-tolerant HKT1;2 allele. Through this work, we aimed to increase HDR efficiency for practical application in a fast crop breeding scenario (Hickey et al., 2019).

RESULTS AND DISCUSSION

The CRISPR/LbCpf1-based geminiviral replicon system is feasible for performing HDR in tomato

To test the hypothesis above, we re-engineered a bean yellow dwarf virus (BeYDV) replicon to supply a high dose of homologous donor templates and used the CRISPR/LbCpf1 system (Zetsche et al., 2015) for DSB formation (Figure 1A and 1B). Two long intergenic regions (LIR) of BeYDV (pLSLR) (Baltes et al., 2014) were cloned in the same orientation with a short intergenic region (SIR) inserted between them, generating an LIR-SIR-LIR amplicon unit. To support the autonomous replication of the amplicon, the Rep/RepA coding sequence was also introduced *in cis* (in the center of the 3' side, SIR-LIR) and transcriptionally driven by the bidirectional promoter activity of the LIR. This cloning strategy interrupted a possible

upstream ORF of Rep/RepA and added an AAA Kozak consensus sequence (Kozak, 1981) upstream of the major ATG of Rep (Supplemental Figure 1A and 1B), thus potentially contributing to increasing the translation of the Rep protein (Barbosa et al., 2013; Zhang et al., 2018). The selection of HDR events was performed with a double selection/screening system based on kanamycin resistance and anthocyanin overproduction (Figure 1A).

To validate our system, the LbCpf1 expression cassette driven by the CaMV 35S promoter and 5'UTR with AtUBI10 intron I (to suppress silencing effects (Christie et al., 2011)), guide RNA scaffolds driven by the AtU6 promoter (Belhaj et al., 2013) and donor templates were cloned into the *de novo*-engineered geminiviral DNA amplicon (Figure 1B) and transformed via *Agrobacterium*-mediated transformation into tomato cotyledon explants. The *de novo*-engineered geminiviral DNA amplicon system exhibited efficient and durable maintenance of circularized DNAs in mature tomato leaves (Supplemental Figure 2). The LbCpf1 system using two guide RNAs for targeting the ANT1 gene, a key transcription factor controlling the anthocyanin pathway, showed a much higher HDR efficiency, of 4.51±0.63% (normalized to an overexpression construct (pANT1^{ox}, Figure 1B)), than the other control constructs, including the "minus Rep" (pRep^{-}) and "minus gRNA" (pgRNA^{-}) constructs. LbCpf1 system-based HDR was visualized by the presence of purple calli and/or shoots (Figure 1C and 1D), and its efficiency was similar to that of a CRISPR/SpCas9-based construct (pTC217) (Cermak et al., 2015) included in the same experiment (Figure 1C) or used in hexaploid wheat with the same scoring method (Gil-Humanes et al., 2017). It is worth noting that the normalized HDR efficiencies reported from this study (see Materials and Methods section) using transformed cell-based efficiency are calculated differently from those reported in the initial work by Čermák and coworkers (2015); the previous authors used the transformed cotyledon-based

efficiency, which is approximately one order of magnitude higher than the cell-based efficiency. The data obtained from this experiment revealed that functional geminiviral replicons were crucial for increasing HDR efficiencies of the Cpf1 complex. This result shows the feasibility of highly efficient HDR in plants using Cpf1 expressed from a geminiviral replicon, thus expanding the choices of molecular scissors for gene targeting in plants.

Favorable physical conditions significantly increase the HDR efficiency of the CRISPR/LbCpf1-based geminiviral replicon system

In seeking suitable physical conditions for *Agrobacterium*-mediated delivery and DSB repair using our HDR tool in tomato somatic cells, we investigated various incubation regimes at early stages posttransformation. Short-day conditions have been shown to have strong impacts on intrachromosomal recombination repair (ICR) in *Arabidopsis* (Boyko et al., 2005). We tested whether the same could be true for the gene targeting approach in tomato. Using various lighting regimes, including complete darkness (DD), short (8 hours light/16 hours dark; 8 L/16 D)- and long (16 L/8 D)-day conditions, we found that the HDR efficiencies achieved under short- and long-day conditions were higher than those under DD conditions in the case of LbCpf1 but not SpCas9 and reached 6.62±1.29% ($p<0.05$, Figure 1E). Considering the similar repair activities observed after DSBs were generated by either of the CRISPR/Cas systems, it was quite difficult to explain why the light conditions only affected LbCpf1-based HDR in this experiment compared to the dark treatment. There must be unknown mechanism(s) that facilitate LbCpf1-mediated HDR in a light-dependent manner.

Temperature is an important factor controlling ICR (Boyko et al., 2005), CRISPR/Cas9-based targeted mutagenesis in plants (LeBlanc et al., 2018), and CRISPR/Cpf1-based HDR in

zebrafish and *Xenopus* by controlling genome accessibility (Moreno-Mateos et al., 2017). Pursuing the approach for the improvement of HDR, we compared the HDR efficiencies of the pHR01 and pTC217 systems subjected to various temperature treatments under an 8 L/16 D photoperiod, since the two nucleases (SpCas9 and LbCpf1) may respond differently. Our data revealed that within a temperature range of 19-31°C, the somatic HDR efficiency increased with increasing temperature (Figure 1F). Notably, at 31°C, LbCpf1 showed an HDR efficiency (9.80±1.12%) that was more than 2-fold higher than that of SpCas9 ($p<0.05$) and was nearly twice that of a similar system in hexaploid wheat (Gil-Humanes et al., 2017) as well as an LbCpf1-based T-DNA tool in rice (Li et al., 2018). The results supported the principle of stress-stimulated HDR in plants reported by Boyko and coworkers (2005). The ease of LbCpf1at genome accessibility at high temperatures (Moreno-Mateos et al., 2017) in combination with the ability to repeatedly cut at the target sites (Zetsche et al., 2015) may explain the higher HDR efficiency of LbCpf1 compared to that of SpCas9. In addition, Malzahn and coworkers (2019) recently reported dependency of Cpf1 cleavage activity on temperature. Interestingly, the LbCpf1 complex was shown to be highly active only at high temperatures (i.e., more than 29°C), which partially explains the higher HDR efficiencies observed at high temperatures in this experiment. Briefly, a comparison of data on plant HDR between Cas9- and Cpf1-based systems at different temperatures and under short-day conditions is presented to reveal the best conditions for plant HDR improvement.

A multiple-replicon system outperformed the single-replicon system in HDR-based GE.

The size of viral replicons has been shown to be inversely correlated with their copy numbers (Baltes et al., 2014; Suarez-Lopez and Gutierrez, 1997). In an approach to overcome the

replicon size limitation, we designed and tested the novel idea of using a T-DNA system that potentially produces multiple replicons (Figure 2A, and Supplemental Figure 3). Compared to pHR01, a multiple-replicon system designed to release donor templates from replicon 2 (MR02) but not replicon 1 (MR01) showed a significant increase in the HDR efficiency by 30% and reached up to 12.79±0.37% (Figure 2B and Supplemental Table 1). Temporal evaluation of donor template levels between the HDR tools showed significantly higher levels of MR02 at 3 days posttransformation (dpt) compared to those of pHR01 and MR01 (Figure 2C). Higher donor template levels were available while CRISPR/Cas was generating DSBs at early times after transformation (3 dpt, MR02, Figure 2C) but not later (6 dpt, MR01, Figure 2C). Under the same conditions and calculation methods, the combination of our multiple replicons with LbCpf1 significantly increased HDR efficiencies by 3-4-fold compared to those of the Cas9-based replicon systems. We also confirmed the release of three circularized replicons from the single vector used in this work (Figure 2D) by PCR amplification using circularized replicon-specific primers (Supplemental Table 2).

In another test of the multiple replicon system, we overexpressed two key proteins involved in the plant HDR pathway from the replicon 1 site. Either SlRAD51 (Solyc07g017540.2) or SlRAD54 (Solyc04g056400.2) was overexpressed with the multiple replicon tools (MR03 and MR04) (Figure 2A). Surprisingly, even when the donor template level of MR03 or MR04 was nearly twice that of MR01 (Figure 2C), the HDR efficiency was not significantly different in the case of MR03 and was even significantly lower for MR04 (Figure 2B and Supplemental Table 1). Overexpression of SlRAD54 might increase the displacement of SlRAD51 from SlRAD51-bound dsDNAs at the early stage of HDR initiation (Petukhova et al., 1999), thereby suppressing HDR to some extent in the case of MR04 (Figure 2B). Overexpression of either

SlRAD51 or SlRAD54 increased geminiviral replication (replicon 2 and 3) several-fold compared to the control (MR02), confirming the positive roles of these proteins in geminivirus replication in a homologous recombination manner, as reported elsewhere (Kaliappan et al., 2012; Richter et al., 2016; Suyal et al., 2013) The data also revealed a temporal difference in the maximal peaks of replicon 1 and 2 because replicon 1 was not accompanied by a Rep/RepA expression cassette.

The multiple replicon system may provide more flexible choices for expressing multiple donor templates/genes/genetic tools in plant cells with temporally controllable copy levels without incurring an expression penalty from excess replicon sizes up to 18 kb (size of replicon 3 released by MR03). The validation of the multireplicon system provides an excellent alternative for genetic engineering in plants in addition to applications in plant genome editing. If we carefully design and clone multiple donor templates or gene expression cassettes into the multireplicons, we can control donor templates/gene doses without incurring penalties from excessing replicon size limitations.

True ANT1 HDR events occurred at high frequency

To verify HDR repair events, PCR analyses were conducted using primers specific for the left (UPANT1-F1/NptII-R1) and right (ZY010F/TC140R) (Figure 1A; Supplemental Table 3 and 4) junctions employing genomic DNAs extracted from derived HDR events (independently regenerated purple plants or genome-edited generation 0 (GE0)) (Figure 3A, Supplemental Figure 4). For pHR01, all (16/16) of the independent events showed the expected band for right junction integration, and 10/16 independent events showed the expected band for left junction repair (Figure 3B). The PCR products were sequenced to identify junction sequences.

A majority of the events (11/16) showed sequences corresponding to perfect right arm integration through HDR repair, and 5/16 events showed a combination of HDR and NHEJ repair with an NHEJ fingerprint at the 5' terminus of the pNOS sequence (Supplemental Figure 5A, with event C1.8 highlighted in blue) or even RB integration at the left junction boundary (Supplemental Figure 6). All of the sequences amplified from the left junctions showed perfected DNA sequence exchange via the HDR pathway (Supplemental Figure 5B). The results obtained in these analyses revealed the common features of products repaired via HDR pathways in plant somatic cells reported elsewhere in dicots(Butler et al., 2016; Cermak et al., 2015; Dahan-Meir et al., 2018) and monocots (Gil-Humanes et al., 2017; Li et al., 2018), regardless of whether a T-DNA or geminiviral replicon system was involved. More importantly, 15 out of 16 events showed no amplification of circularized forms of the DNA replicon, and even the replicon-carrying events lost this replicon after long-term growth in greenhouse conditions (data not shown), indicating that these plants were free of the replicon (Figure 3B). The absence of the replicon might be hypothetically explained by reverse construction of the donor template (Figure 1B), leading to the opposite arrangement of the LIR forward promoter sequence against a 35S promoter sequence (LIR-p35S orientation interference), which triggers a silencing mechanism in plant cells in later stages. This possibility was later supported by the appearance of replicons in the majority of plants regenerated using other replicon systems without LIR-p35S orientation interference.

The HDR allele was stably inherited in offspring by self-pollination as well as backcrossing

To confirm stable heritable edits, we grew genome-edited generation 1 (GE1) plants (Figure 3C) obtained from the self-pollination of LbCpf1-based HDR GE0 events and identified a

segregating population with a purple phenotype (Supplemental Table 5) similar to the segregating profiles shown by Čermák and coworkers (2015). PCR analyses of the segregating plants showed inheritance of the edited allele (Figure 3D and Supplemental Figure 7). The offspring segregated from the #C1.4 event were analyzed in detail. Five dark purple plants (C1.4.1-C1.4.5, homozygous for the ANT1 HDR-edited allele, Supplemental Figure 8), six pale purple plants (C1.4.30-C1.4.35, heterozygous for the ANT1 HDR-edited allele, Supplemental Figure 8), and two wild-type-like plants did not contain the HDR-edited allele, as expected (Figure 3D, predicted results correlated with phenotypes). The dark purple plants showed PCR amplification from the replaced allele but no amplification of the wild-type allele when PCR was performed using primers flanking the editing site (Figure 1A). In contrast, heterozygous and wild-type plants showed a band corresponding to the wild-type allele. Further assessment indicated that the GE2 offspring of the homozygous GE1 plants were all dark purple, and the back-crossed (to WT female as pollen acceptors) BC1F1 generation all showed the pale purple phenotype (Supplemental Figure 8), suggesting the feasibility of recovering the parental genetic background via backcrossing in cases of unexpected modification, including off-target effects. Sanger sequencing revealed perfect inheritance of the HDR-edited allele from the GE0 generation of event C1.4 (Supplemental Figure 9) to its homozygous offspring. These data also showed no amplification of circular forms of the DNA replicon (Figure 3D and Supplemental Figure 7), indicating that the GE1 plants were also free of the replicons.

Practical successful editing by HDR using marker-free approaches

To show the applicability of our HDR system to practical plant genome editing, we sought to use it to edit a potentially agronomic trait, and salinity tolerance was chosen as the target trait. High-affinity K^+ Transporter 1;2 (HKT1;2) plays an important role in the maintenance of K+ uptake under salt stress (Ali et al., 2012). Salinity tolerance was determined by a single N/D variant (N217D in tomato) in the pore region of HKT1;2, which determines selectivity for Na+ and K+ (Ali et al., 2016). We succeeded in generating a heterozygous but perfect HDR GE0 event to produce the salt-tolerant allele (N217D) (Ali et al., 2016) (Figure 4A, Supplemental Table 6) according to the analysis of 150 events (~0.66%) using our system with a *HKT1;2* gene donor template that included neither an antibiotic selection marker nor an ANT1 color marker (Figure 4B). The CRISPR/LbCpf1 system was very effective for NHEJ repair because it generated indel mutation rates of up to 72% in multiple mutation patterns decomposed by ICE Synthego software (Hsiau et al., 2019) (Supplemental Figure 10A and B), in which most of the events resulted in 47-97% cells carrying indel sequences (ICE score, Supplemental Table 7). In comparison with the first report on the marker-free gene targeting of the CRTISO allele (Dahan-Meir et al., 2018), this efficiency was much lower, possibly due to (1) lower cutting activity (note the indel rates in Supplemental Table 7), (2) a different target site context or (3) the use of a different strategy to express Rep/RepA (Dahan-Meir and coworkers used a replicon tool with Rep expression driven by a CaMV35S promoter from outside of LIR-SIR-LIR boundary), or to unknown reasons associated with the CRTISO alleles, as claimed by the authors, or all of the above-mentioned factors. We used a similar replicon tool to that reported by Dahan-Meir and coworkers (2018) for ANT1 targeting via the HDR pathway in this study but obtained significantly lower HDR efficiencies than were obtained with the pHR01 tool (data not shown).

The editing event involving the D217 allele resulted in a normal morphology (Figure 4C) and normally set fruits (Supplemental Figure 11) compared to WT. It should be noted that the mutated nucleotide (A to G) of *HKT1;2* is not accessible by any currently known base editor (BE), including xCas9-ABE (Hu et al., 2018), highlighting the significance of HDR-based genome editing. We tested the self-pollinated GE1 generation of the plants obtained from the event and observed up to 100 mM NaCl tolerance at the germination stage (Figure 5A) in homozygous as well as heterozygous plants. The salt-tolerant plants showed a 3-4-day delay in germination compared to the mock controls but grew normally in NaCl-containing medium (Figure 5A) and later fully recovered in soil (Figure 5B). Screening for the presence of HDR allele(s) in the tested plants via the cleaved amplified polymorphic sequence (CAPS) method showed allele segregation following Mendelian rules (Figure 5C). The true HKT1;2 N217D HDR alleles in the GE1 plants were ultimately confirmed by Sanger sequencing. Furthermore, we successfully generated HDR-based SlEPSPS1 events with an ~1% efficiency using this replicon system without using herbicide for selection (data not shown), thereby validating the feasibility of our replicon systems for practical applications. It is worth noting that most of the elite alleles in plants do not associate with any marker, and hence, a highly efficient marker-free system is in high demand.

Thus, through the application of various approaches, our study showed a large improvement of HDR efficiency in tomato somatic cells. The HDR allele was stably inherited in subsequent generations obtained via self-pollination and backcrossing. The advancement of HDR in somatic cells and the generation of replicon-free HDR-edited plants in the GE0 generation open the door for practical applications of the technique to improve crop traits, with special interest for asexually reproducing crops.

MATERIALS AND METHODS

Construction and cloning of HDR testing systems

The entire design principle and all cloning procedures followed MoClo (Weber et al., 2011) and Golden Gate (Engler et al., 2014) protocols. pLSL.R. Ly was designed by amplifying the long intergenic region (LIR), short intergenic region (SIR) and lycopene marker from the pLSLR plasmid (Cermak et al., 2015) and was cloned following the order shown in Supplemental Figure 2A. Level 2 Golden Gate BpiI restriction sites flanking the pink marker gene (lycopene) were also integrated within the replicon for the cloning of HDR expression cassettes. The release of circularized DNA replicons was validated in tomato leaves (Supplemental Figure 2B) as well as tomato cotyledon explants (data not shown). The pTC147 and pTC217 plasmids (Cermak et al., 2015) were obtained from Addgene and used as a reference. The LbCpf1-based HDR replicons were designed and cloned similarly to the SpCas9-based constructs, with two guide RNAs (LbCpf1_gRNA1 and LbCpf1_gRNA2, Figure 1A). Donor DNAs (ANT1D2) were constructed for the integration of an antibiotic selection marker (NptII) and the insertion of a CaMV 35S promoter to drive overexpression of the ANT1 gene (pANT1^{ox}, Figure 1A). The dual-guide RNA construct was designed by multiplexing the LbCpf1 crRNAs as a tandem repeat of scaffold RNA followed by 23 nt guide RNA sequences. The crRNAs were driven by an AtU6 promoter (Kamoun Lab, Addgene #46968) and terminated by 7-T chain sequences.

Tomato transformation

Our study of HDR improvement was conducted using tomato (Hongkwang cultivar, a local variety) as a model plant. All the binary vectors were transformed into *Agrobacterium*

tumefaciens GV3101 (pMP90) using electroporation. *Agrobacterium*-mediated transformation was used to deliver editing tools to tomato cotyledon fragments (Supplemental Figure 12). Explants for transformation were prepared from 7-day-old cotyledons. Sterilized seeds of the Hongkwang cultivar were grown in MSO medium (half-strength MS medium containing 30 g/L of sucrose, pH 5.8) at 25±2ºC under 16-hour/8=hour light/dark conditions. Seven-day-old seedlings were collected, and their cotyledonary leaves were sliced into 0.2-0.3 cm fragments. The fragments (explants) were pretreated in PREMC medium [MS basal salts, Gamborg B5 vitamins, 2.0 mg/L of Zeatin trans isomer and 0.2 mg/L of indolyl acetic acid (IAA), 1 mM of putrescine and 30 g/L of glucose, pH 5.7] for 1 day. The precultured explants were then pricked and transformed using *A. tumefaciens* GV3101::pMP90 cells carrying HR construct(s).

A. tumefaciens GV3101::pMP90 cells were grown in primary culture overnight (LB containing suitable antibiotics) in a shaking incubator at 30ºC. Agrobacteria were then collected from the culture (OD 0.6-0.8) by centrifugation. The cells were resuspended in liquid ABM-MS (pH 5.2) and 200 µM acetosyringone. Transformation was carried out for 25 min at RT. The explants were then transferred to cocultivation medium containing all of the components in the ABM-MS medium and 200 µM acetosyringone, pH 5.8. The cocultivation plates were kept in the darkness at 25ºC for 2 days, and the explants were then shifted to nonselection medium (NSEL) for 5 days and subcultured in selection medium (SEL5). The nonselection and selection media contained all of the components of the preculture medium as well as 300 mg/L of timentin and 80 mg/L of kanamycin. Subculture of the explants was carried out at 14-day intervals to achieve the best regeneration efficiency. Explants containing purple calli or shoots were then transferred to SEL5R medium (similar to SEL5 but with the zeatin trans isomer concentration reduced to 1.0 mg/L) for further regeneration and/or

elongation. When the shoots were sufficiently long (1.5-3.0 cm), they were transferred to rooting medium (containing all of the components of the elongation medium the except zeatin trans isomer plus 1.0 mg/L IBA) to generate intact plants. The intact plants from the rooting medium were transferred to vermiculite pots to allow them to harden before shifting them to soil pots in a greenhouse with a temperature of 26±2ºC under a 16 h/8 h photoperiod. The experimental treatment of the physical conditions and data collection were conducted as described in Supplemental Figure 12.

HDR efficiency calculation

In a previous report, the HDR efficiency calculated by dividing the number of explants containing at least one purple callus (appearing as a purple spot) by the total number of explants obtained from *Agrobacterium*-mediated transformation reached 12% with the replicon system (Cermak et al., 2015). In the present study, HDR efficiencies were calculated differently by normalization of the purple spot numbers per cotyledon fragment obtained using genome editing constructs to the purple spot numbers per cotyledon fragment counted in case of transformation of the SlANT1 overexpression cassette (pTC147 and pANT1^{ox}, Figure 1B) in the same conditions.

Plant genomic DNA isolation

Tomato genomic DNA isolation was performed using the DNeasy Plant Mini Kit (Qiagen, USA) according to the manufacturer's protocol. Approximately 200 mg of leaf tissue was crushed in liquid nitrogen using a ceramic mortar and pestle and processed with the kit. Genomic DNA was eluted from the mini spin column with 50-80 µl of TE or nuclease-free water.

HDR event evaluation

The assessment of gene targeting junctions was performed by conventional PCR using primers flanking the left (UPANT1-F1/NptII-R1) and right (ZY010F/TC140R (Cermak et al., 2015) (Supplemental Table 3 and 4) junctions and a high-fidelity Taq DNA polymerase (Phusion Taq, Thermo Fisher Scientific, USA) and Sanger sequencing (Solgent, Korea). DNA amplicons and related donor template levels were evaluated by semiquantitative PCR and qPCR (using KAPA SYBR FAST qPCR Kits, Sigma-Aldrich, USA), respectively, using primers specific to only circularized replicons and the donor template. Additionally, the qPCR assays were designed and conducted following MIQE's guidelines, with SlPDS (Solyc03 g123760**)** and SlEF1 (Solyc07 g016150**)** as normalized controls. Analyses of the inherited behavior of the HDR-edited allele were performed with genome-edited generation 1 (GE1) by PCR and Sanger sequencing. Circularized replicons were detected using PCR with the corresponding primers for pHR01 (Supplemental Table 3), multiple replicons (Supplemental Table 2) or pTC217 (Supplemental Table 4).

Statistical analyses

HDR efficiencies were recorded in at least three replicates and were statistically analyzed and plotted using PRISM 7.01 software. In Figure 1C, multiple comparisons of the HDR efficiencies of the other constructs with that of pRep$^-$ were performed by one-way ANOVA (uncorrected Fisher LSD test, n=3, df=2, t=4.4; 4.4 and 1.5 for pTC217; pHR01 and pgRNA$^-$, respectively). In Figure 1E, pairwise comparisons of the HDR efficiencies of pTC217 and pHR01 under the three lighting conditions were performed with Student's t-test (DD: t=1.222, df=4; 8 L/16 D: t=2.424, df=7 and 16 L/8 D: t=3.059, df=4). In Figure 1F, comparisons of the

HDR efficiencies of pTC217 and pHR01 in the various temperature conditions were performed with Student's t-test (19°C: t=2.656, df=2; 25°C: t=3.346, df=2; 28°C: t=2.099, df=5; 31°C: t=4.551, df=2). In Figure 2B, comparisons of the HDR efficiencies of the other multiple replicon tools with pHR01 were performed with Student's test (MR01: t=3.648, df=3; MR02: t=6.041, df=3; MR03: t=2.032, df=3; MR04: t=1.893, df=3).

FUNDING

This work was supported by the National Research Foundation of Korea (Grant NRF 2017R1A4A1015515) and by the Next-Generation BioGreen 21 Program (SSAC, Grant PJ01322601), Rural Development Administration (RDA), Republic of Korea.

AUTHOR CONTRIBUTIONS

T.V.V., V.S. and J.Y.K. designed the experiments; T.V.V., V.S., E.J.K., M.T.T., J.K., Y.W.S., D.T.H.D and M.P. performed the experiments; T.V.V. and J.Y.K. analyzed the results; T.V.V. and J.Y.K. wrote the manuscript.

COMPETING INTERESTS

The authors have submitted a Korean patent application (application no. 10-2018-0007579) based on the results reported in this paper.

ACKNOWLEDGMENTS

We wish to thank Mrs. Jeong Se Jeong and Mrs. Hyun Jeong Kim for their valuable technical support in this study.

REFERENCES

Ali, A., Raddatz, N., Aman, R., Kim, S., Park, H.C., Jan, M., Baek, D., Khan, I.U., Oh, D.H., Lee, S.Y., *et al.* (2016). A Single Amino-Acid Substitution in the Sodium Transporter HKT1 Associated with Plant Salt Tolerance. Plant Physiol *171*, 2112-2126.

Ali, Z., Park, H.C., Ali, A., Oh, D.H., Aman, R., Kropornicka, A., Hong, H., Choi, W., Chung, W.S., Kim, W.Y., *et al.* (2012). TsHKT1;2, a HKT1 homolog from the extremophile Arabidopsis relative Thellungiella salsuginea, shows K(+) specificity in the presence of NaCl. Plant Physiol *158*, 1463-1474.

Baltes, N.J., Gil-Humanes, J., Cermak, T., Atkins, P.A., and Voytas, D.F. (2014). DNA replicons for plant genome engineering. Plant Cell *26*, 151-163.

Barbosa, C., Peixeiro, I., and Romao, L. (2013). Gene expression regulation by upstream open reading frames and human disease. PLoS Genet *9*, e1003529.

Barrangou, R., and Doudna, J.A. (2016). Applications of CRISPR technologies in research and beyond. Nat Biotechnol *34*, 933-941.

Belhaj, K., Chaparro-Garcia, A., Kamoun, S., and Nekrasov, V. (2013). Plant genome editing made easy: targeted mutagenesis in model and crop plants using the CRISPR/Cas system. Plant Methods *9*, 39.

Boyko, A., Filkowski, J., and Kovalchuk, I. (2005). Homologous recombination in plants is temperature and day-length dependent. Mutat Res *572*, 73-83.

Butler, N.M., Baltes, N.J., Voytas, D.F., and Douches, D.S. (2016). Geminivirus-Mediated Genome Editing in Potato (Solanum tuberosum L.) Using Sequence-Specific Nucleases. Front Plant Sci *7*, 1045.

444 Cermak, T., Baltes, N.J., Cegan, R., Zhang, Y., and Voytas, D.F. (2015). High-frequency,
445 precise modification of the tomato genome. Genome Biol *16*, 232.
446 Christie, M., Croft, L.J., and Carroll, B.J. (2011). Intron splicing suppresses RNA silencing
447 in Arabidopsis. Plant J *68*, 159-167.
448 Dahan-Meir, T., Filler-Hayut, S., Melamed-Bessudo, C., Bocobza, S., Czosnek, H., Aharoni,
449 A., and Levy, A.A. (2018). Efficient in planta gene targeting in tomato using geminiviral
450 replicons and the CRISPR/Cas9 system. Plant J *95*, 5-16.
451 Endo, M., Mikami, M., and Toki, S. (2016). Biallelic Gene Targeting in Rice. Plant Physiol
452 *170*, 667-677.
453 Engler, C., Youles, M., Gruetzner, R., Ehnert, T.M., Werner, S., Jones, J.D., Patron, N.J., and
454 Marillonnet, S. (2014). A golden gate modular cloning toolbox for plants. ACS Synth Biol *3*,
455 839-843.
456 Fauser, F., Roth, N., Pacher, M., Ilg, G., Sanchez-Fernandez, R., Biesgen, C., and Puchta, H.
457 (2012). In planta gene targeting. Proc Natl Acad Sci U S A *109*, 7535-7540.
458 Ferguson, D.O., and Alt, F.W. (2001). DNA double strand break repair and chromosomal
459 translocation: lessons from animal models. Oncogene *20*, 5572-5579.
460 Gil-Humanes, J., Wang, Y., Liang, Z., Shan, Q., Ozuna, C.V., Sanchez-Leon, S., Baltes, N.J.,
461 Starker, C., Barro, F., Gao, C., *et al.* (2017). High-efficiency gene targeting in hexaploid wheat
462 using DNA replicons and CRISPR/Cas9. Plant J *89*, 1251-1262.
463 Gutierrez, C. (1999). Geminivirus DNA replication. Cell Mol Life Sci *56*, 313-329.
464 Hanley-Bowdoin, L., Bejarano, E.R., Robertson, D., and Mansoor, S. (2013). Geminiviruses:
465 masters at redirecting and reprogramming plant processes. Nat Rev Microbiol *11*, 777-788.

Hickey, L.T., A, N.H., Robinson, H., Jackson, S.A., Leal-Bertioli, S.C.M., Tester, M., Gao, C., Godwin, I.D., Hayes, B.J., and Wulff, B.B.H. (2019). Breeding crops to feed 10 billion. Nat Biotechnol.

Hsiau, T., Conant, D., Maures, T., Waite, K., Yang, J., Kelso, R., Holden, K., Enzmann, B.L., and Stoner, R. (2019). Inference of CRISPR Edits from Sanger Trace Data. bioRxiv, 251082.

Hsu, P.D., Lander, E.S., and Zhang, F. (2014). Development and applications of CRISPR-Cas9 for genome engineering. Cell *157*, 1262-1278.

Hu, J.H., Miller, S.M., Geurts, M.H., Tang, W., Chen, L., Sun, N., Zeina, C.M., Gao, X., Rees, H.A., Lin, Z., *et al.* (2018). Evolved Cas9 variants with broad PAM compatibility and high DNA specificity. Nature *556*, 57-63.

Hummel, A.W., Chauhan, R.D., Cermak, T., Mutka, A.M., Vijayaraghavan, A., Boyher, A., Starker, C.G., Bart, R., Voytas, D.F., and Taylor, N.J. (2018). Allele exchange at the EPSPS locus confers glyphosate tolerance in cassava. Plant Biotechnol J *16*, 1275-1282.

Jiang, W., Zhou, H., Bi, H., Fromm, M., Yang, B., and Weeks, D.P. (2013). Demonstration of CRISPR/Cas9/sgRNA-mediated targeted gene modification in Arabidopsis, tobacco, sorghum and rice. Nucleic Acids Res *41*, e188.

Jinek, M., Chylinski, K., Fonfara, I., Hauer, M., Doudna, J.A., and Charpentier, E. (2012). A programmable dual-RNA-guided DNA endonuclease in adaptive bacterial immunity. Science *337*, 816-821.

Kaliappan, K., Choudhury, N.R., Suyal, G., and Mukherjee, S.K. (2012). A novel role for RAD54: this host protein modulates geminiviral DNA replication. FASEB J *26*, 1142-1160.

Kozak, M. (1981). Possible role of flanking nucleotides in recognition of the AUG initiator codon by eukaryotic ribosomes. Nucleic Acids Res *9*, 5233-5252.

LeBlanc, C., Zhang, F., Mendez, J., Lozano, Y., Chatpar, K., Irish, V.F., and Jacob, Y. (2018). Increased efficiency of targeted mutagenesis by CRISPR/Cas9 in plants using heat stress. Plant J *93*, 377-386.

Li, S., Li, J., Zhang, J., Du, W., Fu, J., Sutar, S., Zhao, Y., and Xia, L. (2018). Synthesis-dependent repair of Cpf1-induced double strand DNA breaks enables targeted gene replacement in rice. J Exp Bot *69*, 4715-4721.

Mor, T.S., Moon, Y.S., Palmer, K.E., and Mason, H.S. (2003). Geminivirus vectors for high-level expression of foreign proteins in plant cells. Biotechnol Bioeng *81*, 430-437.

Moreno-Mateos, M.A., Fernandez, J.P., Rouet, R., Vejnar, C.E., Lane, M.A., Mis, E., Khokha, M.K., Doudna, J.A., and Giraldez, A.J. (2017). CRISPR-Cpf1 mediates efficient homology-directed repair and temperature-controlled genome editing. Nat Commun *8*, 2024.

Needham, P.D., Atkinson, R.G., Morris, B.A.M., Gardner, R.C., and Gleave, A.P. (1998). GUS expression patterns from a tobacco yellow dwarf virus-based episomal vector. Plant Cell Rep *17*, 631-639.

Nekrasov, V., Staskawicz, B., Weigel, D., Jones, J.D., and Kamoun, S. (2013). Targeted mutagenesis in the model plant Nicotiana benthamiana using Cas9 RNA-guided endonuclease. Nat Biotechnol *31*, 691-693.

Petukhova, G., Van Komen, S., Vergano, S., Klein, H., and Sung, P. (1999). Yeast Rad54 promotes Rad51-dependent homologous DNA pairing via ATP hydrolysis-driven change in DNA double helix conformation. J Biol Chem *274*, 29453-29462.

Puchta, H. (2005). The repair of double-strand breaks in plants: mechanisms and consequences for genome evolution. J Exp Bot *56*, 1-14.

Puchta, H., Dujon, B., and Hohn, B. (1993). Homologous recombination in plant cells is enhanced by in vivo induction of double strand breaks into DNA by a site-specific endonuclease. Nucleic Acids Res *21*, 5034-5040.

Puchta, H., Dujon, B., and Hohn, B. (1996). Two different but related mechanisms are used in plants for the repair of genomic double-strand breaks by homologous recombination. Proc Natl Acad Sci U S A *93*, 5055-5060.

Richardson, C., Moynahan, M.E., and Jasin, M. (1998). Double-strand break repair by interchromosomal recombination: suppression of chromosomal translocations. Genes Dev *12*, 3831-3842.

Richter, K.S., Kleinow, T., and Jeske, H. (2014). Somatic homologous recombination in plants is promoted by a geminivirus in a tissue-selective manner. Virology *452-453*, 287-296.

Richter, K.S., Serra, H., White, C.I., and Jeske, H. (2016). The recombination mediator RAD51D promotes geminiviral infection. Virology *493*, 113-127.

Sapranauskas, R., Gasiunas, G., Fremaux, C., Barrangou, R., Horvath, P., and Siksnys, V. (2011). The Streptococcus thermophilus CRISPR/Cas system provides immunity in Escherichia coli. Nucleic Acids Res *39*, 9275-9282.

Suarez-Lopez, P., and Gutierrez, C. (1997). DNA replication of wheat dwarf geminivirus vectors: effects of origin structure and size. Virology *227*, 389-399.

Suyal, G., Mukherjee, S.K., and Choudhury, N.R. (2013). The host factor RAD51 is involved in mungbean yellow mosaic India virus (MYMIV) DNA replication. Arch Virol *158*, 1931-1941.

Szostak, J.W., Orr-Weaver, T.L., Rothstein, R.J., and Stahl, F.W. (1983). The double-strand-break repair model for recombination. Cell *33*, 25-35.

Townsend, J.A., Wright, D.A., Winfrey, R.J., Fu, F., Maeder, M.L., Joung, J.K., and Voytas, D.F. (2009). High-frequency modification of plant genes using engineered zinc-finger nucleases. Nature *459*, 442-445.

Varga, T., and Aplan, P.D. (2005). Chromosomal aberrations induced by double strand DNA breaks. DNA Repair (Amst) *4*, 1038-1046.

Weber, E., Engler, C., Gruetzner, R., Werner, S., and Marillonnet, S. (2011). A modular cloning system for standardized assembly of multigene constructs. PLoS One *6*, e16765.

Zetsche, B., Gootenberg, J.S., Abudayyeh, O.O., Slaymaker, I.M., Makarova, K.S., Essletzbichler, P., Volz, S.E., Joung, J., van der Oost, J., Regev, A., *et al.* (2015). Cpf1 is a single RNA-guided endonuclease of a class 2 CRISPR-Cas system. Cell *163*, 759-771.

Zhang, H., Si, X., Ji, X., Fan, R., Liu, J., Chen, K., Wang, D., and Gao, C. (2018). Genome editing of upstream open reading frames enables translational control in plants. Nat Biotechnol *36*, 894-898.

Zhang, X., and Mason, H. (2006). Bean Yellow Dwarf Virus replicons for high-level transgene expression in transgenic plants and cell cultures. Biotechnol Bioeng *93*, 271-279.

FIGURE LEGENDS

Figure 1. HDR-based genome editing of the ANT1 locus.

(**A**) Representatives of ANT1 targeting sites and homologous DNA donor template construction. The upstream sequence of the ANT1 locus (middle panel) was selected for targeting by HDR. The kanamycin expression cassette (pNOS-NptII-tOCS) and CaMV 35S promoter were designed to be inserted at a position 142 bp upstream of the ANT1 start codon. The cutting sites of the two guide RNAs used in this study are indicated by two black arrows.

555 The sequences of the gRNAs are shown in the bottom panel. The red arrows show the relative
556 binding sites and orientations of the primers used for analyses of HDR events.

557 (**B**) T-DNA constructs used for HDR improvement experiments. The dual-guide RNA
558 scaffold (2x1 gRNA^{ANT1}) was driven by the *Arabidopsis* U6 promoter core element (75 bp).
559 The LbCpf1 expression cassette was re-engineered to contain the *Arabidopsis* Ubiquitin 1
560 intron I downstream of the CaMV 35S promoter and upstream of LbCpf1 and to be terminated
561 by the CaMV 35S terminator (35S-LbCpf1I-t35S). Red and orange boxes indicate long
562 intergenic regions and short intergenic regions of geminivirus DNA, respectively. The black
563 arrow indicates the relevant binding site and orientation of the RRA-R6 primer for subsequent
564 analyses. The red arrows show the orientation of the ANT1 donor templates.

565 (**C**) Comparison of HDR efficiency between different constructs. Transformed tomato
566 cotyledon fragments were incubated under continuous darkness at 28°C for the first 10 days
567 postwashing.

568 (**D**) Representative photographs of HDR-edited T0 events indicated by purple calli (red
569 arrows) or direct HDR shoot formation (yellow arrow).
570 (**E**) Impact of photoperiod on HDR. The transformed tomato cotyledon fragments were
571 incubated under different lighting regimes at 28°C for the first 10 days postwashing. DD:
572 continuous darkness; 8 L/16 D: 8 hours light/16 hours darkness; 16 L/8 D: 16 hour light/8
573 hours dark.
574 (**F**) HDR efficiencies of the pTC217 and pHR01 constructs obtained at various temperatures.
575 HDR efficiencies were recorded in at least triplicate and were calculated and plotted using
576 PRISM 7.01 software (details of the statistical analyses are described in the Methods section).

577 *: significantly different ($p<0.05$); ns: not significantly different; p values are shown on the
578 top of the bars of (**E**) for comparison. The data in (**C**), (**E**) and (**F**) are represented as the mean
579 ± SEM.

580 **Figure 2. Next-generation multiple replicon tools for HDR improvement.**

581 (**A**) Multireplicon constructs tested for the improvement of HDR over NHEJ. Red and orange
582 boxes indicate long intergenic regions and short intergenic regions of geminiviral DNA,
583 respectively.
584 (**B**) HDR efficiencies obtained using multiple replicons as cargos for the HDR tools. HDR
585 efficiencies were recorded in triplicate four times and were calculated and plotted using
586 PRISM 7.01 software (details of the statistical analyses are described in the Materials and
587 Methods section). p values (pairwise comparisons to pHR01 using Student's test) are shown
588 on the top of the bars. Data are represented as the mean ± SEM.
589 (**C**) Relatively quantified donor template levels at different time points posttransformation by
590 qPCR using ANT1D2 template-specific primers normalized to SlPDS.
591 (**D**) PCR detection of circularized replicons simultaneously released from the MR01 vector.
592 0d, 3d, 6d and 9d: samples collected at 0, 3, 6 and 9 days posttransformation with
593 *Agrobacterium* carrying MR01. The primer pairs used in PCR to detect circularized replicons
594 are shown in Supplemental Figure 3B, bottom panel, and Supplemental Table 2.

595 **Figure 3. Analyses of HDR-edited plants.**

596 (**A**) Representative HDR-edited plants in greenhouse conditions and their fruits. Scale bars = 1
597 cm.
598 (**B**) PCR analysis data of representative HDR-independent events. P: pHR01 plasmid isolated
599 from Agrobacteria; L: 1 kb ladder; N: water control; WT: wild-type tomato Hongkwang; C1.1,

C1.2, C1.3, C1.8: independent LbCpf1-based HDR GE0 events. ANT1 control products were PCR amplified using the TC140F and TC140R primers (Figure 1A) flanking the upstream region of the ANT1 gene.

(**C**) Generation 1 of HDR-edited events (GE1). GE1 plants (left) germinated in soil in pots in comparison with wild-type plants (right). Scale bar = 1 cm.

(**D**) PCR analysis data of GE1 offspring resulting from C1.4 events. P: pHR01 plasmid isolated from Agrobacteria; L: 1 kb ladder; N: water control; WT: wild-type tomato Hongkwang; C1.4.1, C1.4.2, C1.4.3, C1.4.4 and C1.4.5: GE1 plants showing dark purple color obtained from the self-pollination of plants from the C1.4 event. ANT1 control products were PCR amplified using the TC140F and TC140R primers (Figure 1A) flanking the upstream region of the ANT1 gene.

Figure 4. HKT1;2 N217D allele editing by HDR using the CRISPR/Cpf1-based replicon system.

(**A**) Sanger sequencing of event #C156. Sequence alignment shows the perfectly edited HKT1;2 N217 to D217 allele with the WT allele as a reference. The nucleotides highlighted in the discontinuous red boxes correspond to intended modifications for N217D, PAM and core sequences (to avoid recutting).

(**B**) HDR construct layout for HKT1;2 editing. There is neither selection nor a visible marker integrated into the donor sequence. The *Npt*II marker was used for the enrichment of transformed cells.

(**C**) Morphology of the HKT1;2 N217D edited event compared to its parental WT in greenhouse conditions. Scale bar = 1 cm.

Figure 5. Evaluation of the GE1 offspring of the HKT1;2 N217D HDR event.

(**A**) Salinity tolerance test at the germination stage using NaCl. Left panel: GE1 plants obtained from self-pollination of the plants obtained from event #C156; right panel: WT control. Bar=1 cm.

(**B**) Salt-tolerant plants (right panel) growing in soil showed normal growth compared to WT (left panel). hm=homozygous for the HKT1;2 N211D allele; ht=heterozygous for the HKT1;2 N217D allele. Bar=1 cm.

(**C**) Screening for the presence of HDR allele(s) in the tested plants via the cleaved amplified polymorphic sequence (CAPS) method. PCR amplification using primers flanking the targeted region was conducted. The PCR products were digested with the BpiI enzyme and resolved in a 1% agarose gel. P: Plasmid control; L: 1 kb ladder; WT: wild-type sample; Leaf 1, Leaf 2 and Leaf 3: samples collected from three different positions (angles) on the C156 plants. 1-9: GE1 plants of C156.

LIST OF SUPPLEMENTAL TABLES

Supplemental Table 1. The increase in HDR by multiple replicon systems

Supplemental Table 2. Primers for detecting circularized replicons released by MR01 and pHR01

Supplemental Table 3. Primers for LbCpf1-based HR event analyses

Supplemental Table 4. Primers for SpCas9-based HR event analyses

Supplemental Table 5. Phenotypic segregation of self-pollinated offspring resulting from LbCpf1-based HDR events.

Supplemental Table 6. Summary of the *SlHKT1;2* HDR experiment.

643 Supplemental Table 7. Indel mutation rates among *HKT12* samples decomposed by ICE
644 Synthego software

645 **LIST OF SUPPLEMENTAL FIGURES**

646 **Supplemental Figure 1. Reengineering of the BeYDV Rep coding sequence used in the**
647 **study.**

648 (**A**) Reverse complement view of the LIR-Rep/RepA-SIR sequence isolated from pLSLR.

649 (**B**) Reverse complement view of the LIR-Rep/RepA-SIR sequence in the *de novo*-engineered
650 replicon used in this study.

651 Upper red font sequences: LIR; bottom red font sequences: SIR; purple sequences: Rep/RepA;
652 green font: upstream ORF sequence (uORF); the light blue sequence TCCCAAA was inserted by
653 cloning to interrupt uORF and add the Kozak preference sequence.

654 **Supplemental Figure 2. The *de novo*-engineered geminiviral amplicon (named pLSL.R. Ly)**
655 **and its replication in tomato.**

656 (**A**) Map of pLSL.R.Ly. The DNA amplicon is defined by its boundary sequences (long
657 intergenic region, LIR) and a terminated sequence (short intergenic region, SIR). The
658 replication-associated protein (Rep/RepA) is expressed from the LIR promoter sequence. All of
659 the expression cassettes of HDR tools were cloned into the vector by replacing the red marker
660 (Lycopene) using a pair of type IIS restriction enzymes (BpiI, flanking ends are TGCC and
661 GGGA). Left (LB) and right (RB) denote the borders of a T-DNA.
662 (**B**) Circularized DNA detection in tomato leaves infiltrated with pLSL.R. Ly compared to those
663 infiltrated with pLSLR. Agrobacteria containing the plasmids were infiltrated into tomato leaves

(Hongkwang cultivar), and infiltrated leaves were collected at 6, 8 and 11 dpi and used for the detection of circularized DNAs. N: water; P1: positive control for pLSL.R. Ly; positive control for P2: pLSLR; Cx: Control samples collected at x dpi; Ixy: infiltrated sample number y collected at x dpi; I11 V: sample collected from leaves infiltrated with pLSLR at 11 dpi. PCR products obtained using primers specific to GAPDH were used as loading controls.

Supplemental Figure 3. Schematic representation of the system and the released forms of the MR01 multiple replicon system.

Upper panel: The design for the general construction of multiple replicon complexes included three LIR and three SIR sequences. Middle panel: Representative arrangement of the MR01 tool. The donor template was cloned in one replicon, and the other components for inducing DSBs were located the other replicon. Bottom panel: Three replicons would be formed from the MR01. Primer pairs for detecting circularized replicon 1 (Upr1/pCf. ANT1-R4), replicon 2 (RRA-R2/35S-R4), and replicon 3 (RRA-R2/pCf. ANT1-R4) are indicated in the map of each replicon.

Supplemental Figure 4. Morphological appearance of GE0 plants

Supplemental Figure 5. Sanger sequencing data to confirm donor exchanges.

(**A**) Right junction.

(**B**) Left junction. C1.1, C1.2, C1.3, C1.8, C1.11, C1.12, and C1.17: Independent LbCpf1-based HDR GE0 events

Supplemental Figure 6. Error-prone repair combining HDR and NHEJ in event #C1.3.

The right junctions (amplified by ZY010F/TC140R) of the events were confirmed to be perfectly adapted to HDR repair (Supplemental Figure 5A), but the left junction could not be amplified

(using the UPANT1-F1/NptII-R1 primer pair, Figure 1A). Sequencing of the left junction region showed a ligation event between the RB of the T-DNA and the 3' break in the upstream ANT1 promoter sequence via NHEJ. Red dotted line: ligation boundary.

Supplemental Figure 7. PCR analyses of GE1 plants obtained from GE0 LbCpf1-based HR events.

P: pHR01 plasmid isolated from Agrobacteria; L: 1 kb ladder; N: water control; WT: wild-type Hongkwang; C1.6.1-C1.6.5: GE1 offspring of event C1.6.; C1.9.1: GE1 offspring of event C1.9; C1.10.1 and C1.10.2: GE1 offspring of event C1.10; C1.11.1-C1.11.4: GE1 offspring of event C1.11; C1.12.1-C1.12.5: GE1 offspring of event C1.12; C1.14.1-C1.14.4: GE1 offspring of event C1.14; C1.15.1 and C1.15.2: GE1 offspring of event C1.15; C1.16.1-C1.16.4: GE1 offspring of event C1.16.

Supplemental Figure 8. Morphological appearance of GE1 plants

Supplemental Figure 9. Analyses of left and right junction sequences of GE1 plants.

Sanger sequencing data to confirm donor exchanges for the right (**A**) and left (**B**) junctions of the GE1 plants are presented.

Supplemental Figure 10. Analyses of indel mutations in HKT12 events.

(A) Alignment of raw sequences obtained from Sanger sequencing. 18/25 events (highlighted in yellow) showed strong double peaks indicating single/biallelic mutations. Six out of 25 events showed clear biallelic mutations. C77 showed weak (30%) double peaks. C83 and C105 showed large truncations. (B) Decomposed sequence of event #C53 obtained with ICE Synthego software.

706 **Supplemental Figure 11. Morphology of the heterozygous HKT12 D217 event in a mature**
707 **stage**

708 A plant resulting from the HKT12 D217 event (right) shows a normal morphology and fruit
709 setting compared to the parental plant (left). Scale bars = 2 cm.

710 **Supplemental Figure 12. Timeline and contents of the *Agro*-mediated transformation**
711 **protocol used in this work.**

712 The step-by-step protocol is presented with each number in the circles indicating the number of
713 days after seed sowing (upper panel), and the treatments used in each step are shown in the lower
714 panel.

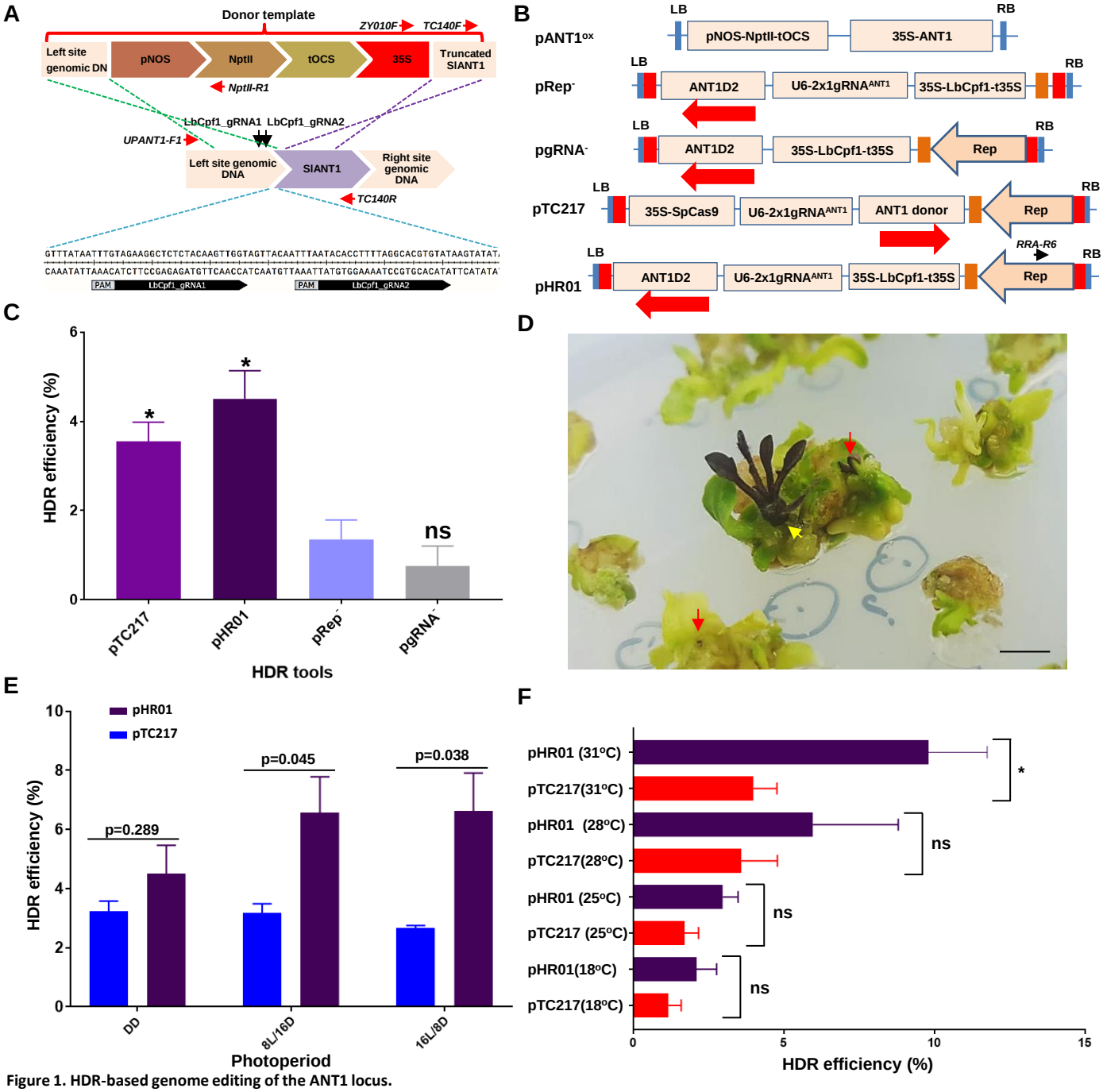

Figure 1. HDR-based genome editing of the ANT1 locus.

(**A**) Representatives of ANT1 targeting sites and homologous DNA donor template construction. The upstream sequence of the ANT1 locus (middle panel) was selected for targeting by HDR. The kanamycin expression cassette (pNOS-NptII-tOCS) and CaMV 35S promoter were designed to be inserted at a position 142 bp upstream of the ANT1 start codon. The cutting sites of the two guide RNAs used in this study are indicated by two black arrows. The sequences of the gRNAs are shown in the bottom panel. The red arrows show the relative binding sites and orientations of the primers used for analyses of HDR events.

(**B**) T-DNA constructs used for HDR improvement experiments. The dual-guide RNA scaffold (2x1 gRNA^{ANT1}) was driven by the *Arabidopsis* U6 promoter core element (75 bp). The LbCpf1 expression cassette was re-engineered to contain the *Arabidopsis* Ubiquitin 1 intron I downstream of the CaMV 35S promoter and upstream of LbCpf1 and to be terminated by the CaMV 35S terminator (35S-LbCpf1I-t35S). Red and orange boxes indicate long intergenic regions and short intergenic regions of geminivirus DNA, respectively. The black arrow indicates the relevant binding site and orientation of the RRA-R6 primer for subsequent analyses. The red arrows show the orientation of the ANT1 donor templates.

(**C**) Comparison of HDR efficiency between different constructs. Transformed tomato cotyledon fragments were incubated under continuous darkness at 28°C for the first 10 days postwashing.

(**D**) Representative photographs of HDR-edited T0 events indicated by purple calli (red arrows) or direct HDR shoot formation (yellow arrow).

(**E**) Impact of photoperiod on HDR. The transformed tomato cotyledon fragments were incubated under different lighting regimes at 28°C for the first 10 days postwashing. DD: continuous darkness; 8 L/16 D: 8 hours light/16 hours darkness; 16 L/8 D: 16 hour light/8 hours dark.

(**F**) HDR efficiencies of the pTC217 and pHR01 constructs obtained at various temperatures.

HDR efficiencies were recorded in at least triplicate and were calculated and plotted using PRISM 7.01 software (details of the statistical analyses are described in the Methods section). *: significantly different ($p<0.05$); ns: not significantly different; p values are shown on the top of the bars of (**E**) for comparison. The data in (**C**), (**E**) and (**F**) are represented as the mean ± SEM.

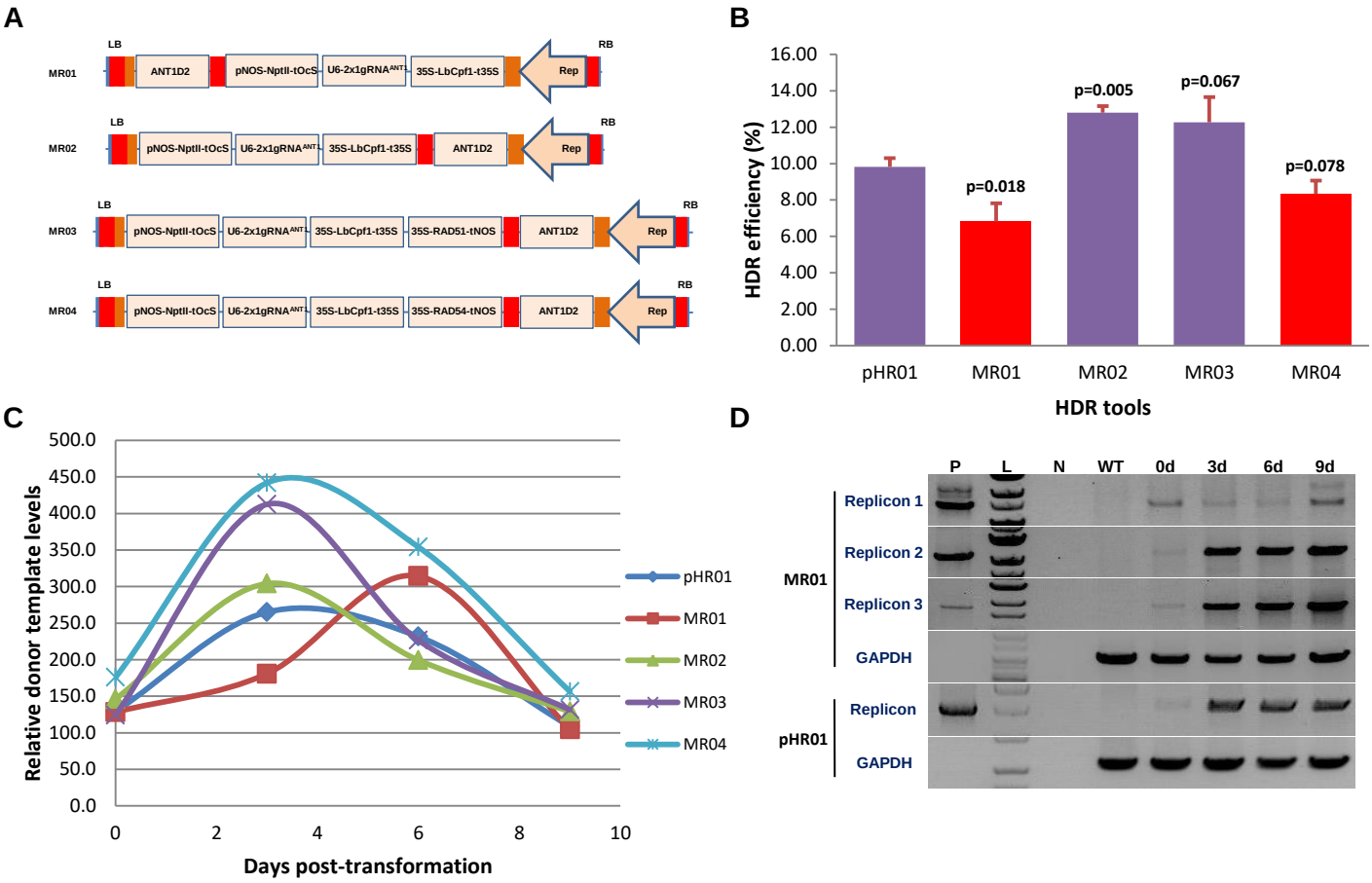

Figure 2. Next-generation multiple replicon tools for HDR improvement.

(**A**) Multireplicon constructs tested for the improvement of HDR over NHEJ. Red and orange boxes indicate long intergenic regions and short intergenic regions of geminiviral DNA, respectively.

(**B**) HDR efficiencies obtained using multiple replicons as cargos for the HDR tools. HDR efficiencies were recorded in triplicate four times and were calculated and plotted using PRISM 7.01 software (details of the statistical analyses are described in the Materials and Methods section). p values (pairwise comparisons to pHR01 using Student's test) are shown on the top of the bars. Data are represented as the mean ± SEM.

(**C**) Relatively quantified donor template levels at different time points posttransformation by qPCR using ANT1D2 template-specific primers normalized to SlPDS.

(**D**) PCR detection of circularized replicons simultaneously released from the MR01 vector. 0d, 3d, 6d and 9d: samples collected at 0, 3, 6 and 9 days posttransformation with *Agrobacterium* carrying MR01. The primer pairs used in PCR to detect circularized replicons are shown in Supplemental Figure 3B, bottom panel, and Supplemental Table 2.

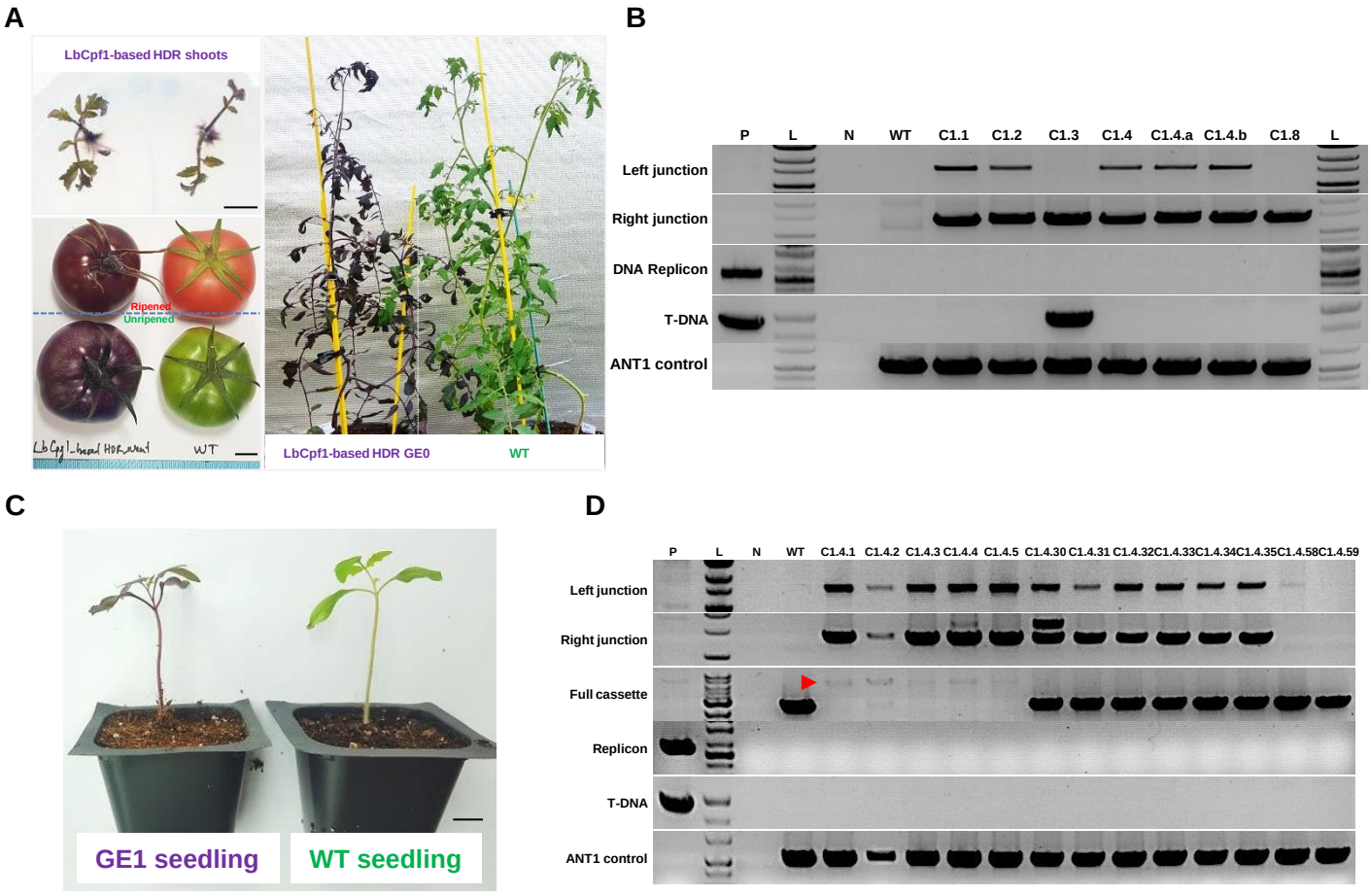

Figure 3. Analyses of HDR-edited plants.

(**A**) Representative HDR-edited plants in greenhouse conditions and their fruits. Scale bars = 1 cm.

(**B**) PCR analysis data of representative HDR-independent events. P: pHR01 plasmid isolated from Agrobacteria; L: 1 kb ladder; N: water control; WT: wild-type tomato Hongkwang; C1.1, C1.2, C1.3, C1.8: independent LbCpf1-based HDR GE0 events. ANT1 control products were PCR amplified using the TC140F and TC140R primers (Figure 1A) flanking the upstream region of the ANT1 gene.

(**C**) Generation 1 of HDR-edited events (GE1). GE1 plants (left) germinated in soil in pots in comparison with wild-type plants (right). Scale bar = 1 cm.

(**D**) PCR analysis data of GE1 offspring resulting from C1.4 events. P: pHR01 plasmid isolated from Agrobacteria; L: 1 kb ladder; N: water control; WT: wild-type tomato Hongkwang; C1.4.1, C1.4.2, C1.4.3, C1.4.4 and C1.4.5: GE1 plants showing dark purple color obtained from the self-pollination of plants from the C1.4 event. ANT1 control products were PCR amplified using the TC140F and TC140R primers (Figure 1A) flanking the upstream region of the ANT1 gene.

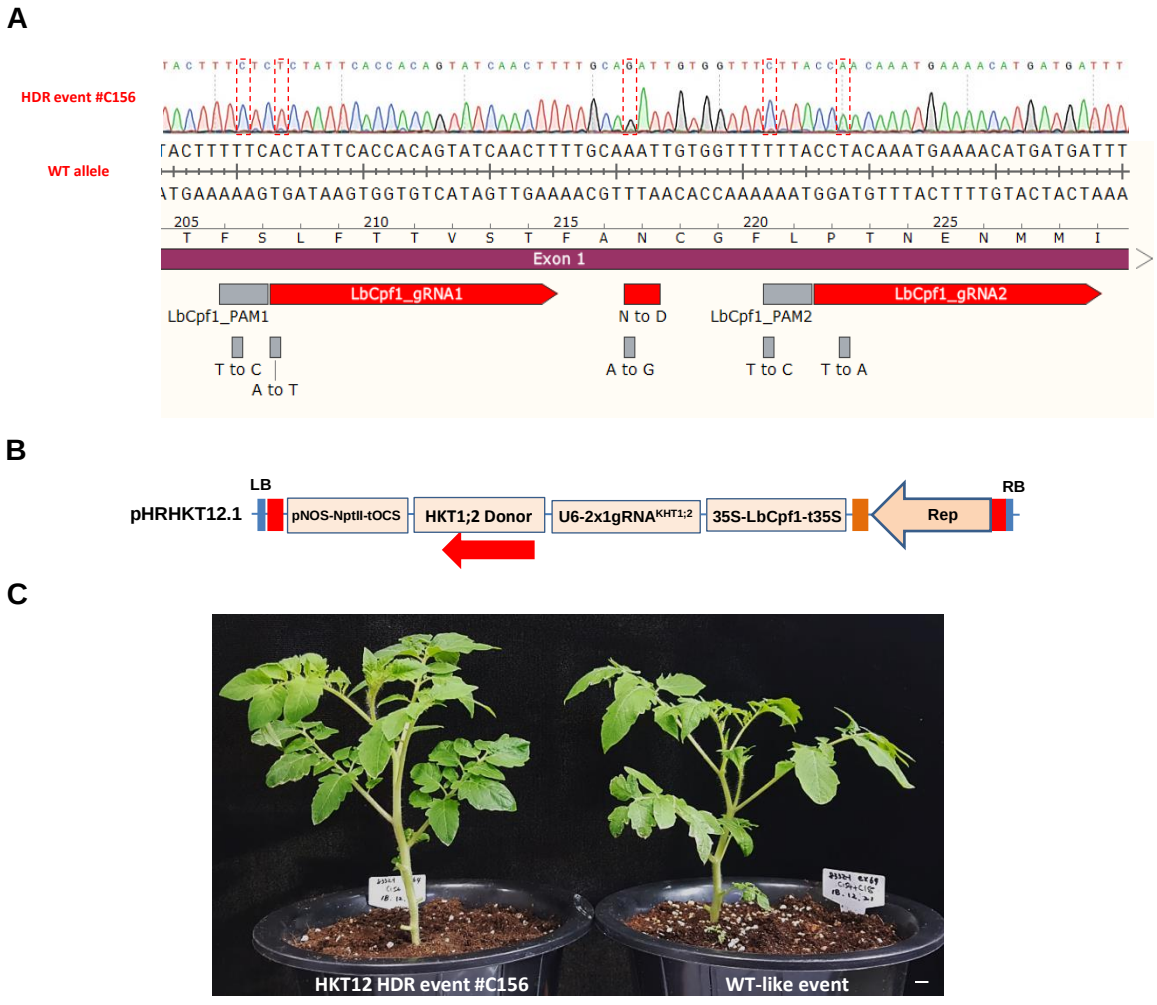

Figure 4. HKT1;2 N217D allele editing by HDR using the CRISPR/Cpf1-based replicon system.
(**A**) Sanger sequencing of event #C156. Sequence alignment shows the perfectly edited HKT1;2 N217 to D217 allele with the WT allele as a reference. The nucleotides highlighted in the discontinuous red boxes correspond to intended modifications for N217D, PAM and core sequences (to avoid recutting).
(**B**) HDR construct layout for HKT1;2 editing. There is neither selection nor a visible marker integrated into the donor sequence. The *Npt*II marker was used for the enrichment of transformed cells.
(**C**) Morphology of the HKT1;2 N217D edited event compared to its parental WT in greenhouse conditions. Scale bar = 1 cm.

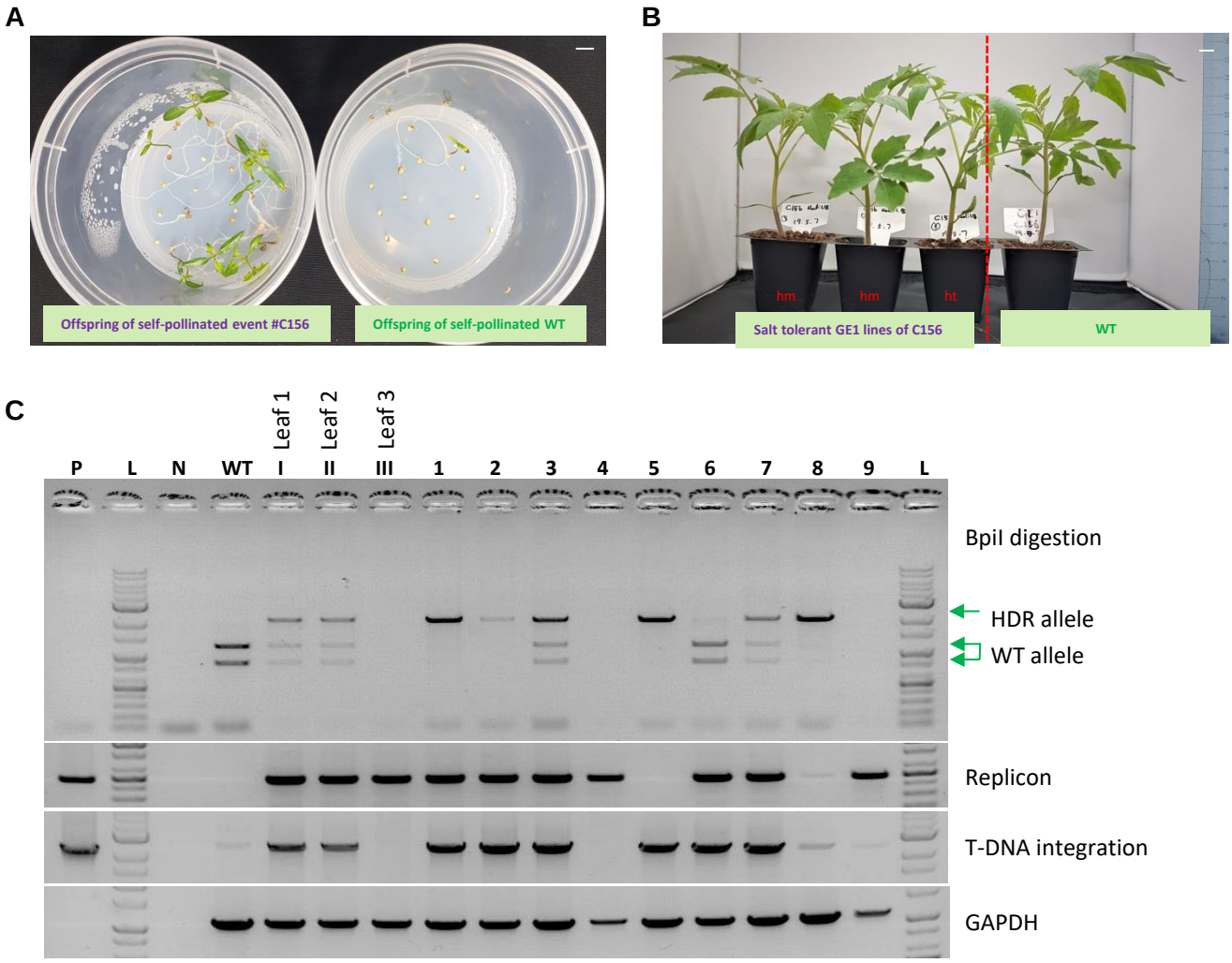

Figure 5. Evaluation of the GE1 offspring of the HKT1;2 N217D HDR event.

(**A**) Salinity tolerance test at the germination stage using NaCl. Left panel: GE1 plants obtained from self-pollination of the plants obtained from event #C156; right panel: WT control. Bar=1 cm.

(**B**) Salt-tolerant plants (right panel) growing in soil showed normal growth compared to WT (left panel). hm=homozygous for the HKT1;2 N211D allele; ht=heterozygous for the HKT1;2 N217D allele. Bar=1 cm.

(**C**) Screening for the presence of HDR allele(s) in the tested plants via the cleaved amplified polymorphic sequence (CAPS) method. PCR amplification using primers flanking the targeted region was conducted. The PCR products were digested with the BpiI enzyme and resolved in a 1% agarose gel. P: Plasmid control; L: 1 kb ladder; WT: wild-type sample; Leaf 1, Leaf 2 and Leaf 3: samples collected from three different positions (angles) on the C156 plants. 1-9: GE1 plants of C156.

A

GAGGGTCGTACGAATAATTCGTATCCAACGGAAATACCTGATACAATATACGCTCCATCAAATACCATCACATCGTAT
ATGCTTTTATAGTGTGAACACCTTTAACCCTAGTGGGCGGGAAATTTTCTACTTTAAATCTGGACCGCTCGTGCTAA
AGCACTCGCGATAAGGGGGGGCCACGCCGGTAATATTAAATTCGGCGTGGGCCCCCCCTTGTCGCAAAGACTTCG
TCTTTAAGTAAATTCCACGTCATTTTCCACTATCTATTAAAATGACCAAAATACCCCTGCCTCCATGCCTCCACGCCG
GTTATAAGATAGAGTTTGAGGCAACCCCTCGGAGTCACAACAACATGCCTTCTGCTAGTAAGAACTTCAGACTCCA
ATCTAAATATGTTTTCCTTACCTATCCCAAGTGCTCATCTCAAAGAGATGATTTATTCCAGTTTCTCTGGGAGAAACT
CACACCTTTTCTTATTTTCTTCCTTGGTGTTGCTTCTGAGCTTCATCAAGATGGCACTACCCACTATCATGCTCTTCTC
CAGCTTGATAAAAAAACCTTGTATTAGGGATCCTTCTTTTTTCGATTTTGAAGGAAATCACCCTAATATCCAGCCAGCT
AGAAACTCTAAACAAGTCCTTGATTACATATCAAAGGACGGAGATATTAAAACCAGAGGAGATTTCCGAGATCATA
AGGTTTCTCCTCGCAAATCTGACGCACGATGGAGAACTATTATCCAGACTGCAACGTCTAAGGAGGAATATCTTGA
CATGATCAAGGAAGAATTCCCTCATGAATGGGCAACAAAGCTTCAATGGCTGGAATATTCAGCCAACAAATTATTC
CCTCCACAACCTGAACCGTATGTGTCGCCCTTCACAGAATCAGATCTTCGCTGCCACGAAGATCTACACTCCTGGA
GGGAAACCCATCTATACCATGTAAGCATAGACGCTTATACTTACATACATCCTGTCTCATACCAACAAGCTCAATCTG
ACCTTGAATGGATGGCCGATTTAACAAGGACAATGGAAGGAATGGAATCCGACACCCCAGCCTCTACATCTGCGG
ACCAACTCGTACCGGAAAGACCACCTGGGCTAGAAGTCTCGGACGACACAACTATTGGAACGGTACCATCGATTT
CACCAACTACGATGAACACGCCACCTATAATATCATCGACGACATCCCCTTCAAGTTCGTCCCATTGTGGAAGCAAT
TAATAGGTTGCCAGTCTGATTTCACTGTCAACCCTAAATATGGAAAAAAGAAGAAAATAAAAGGTGGGATCCCTTC
TATAATTCTTTGCAATCCTGACGAAGACTGGATGTTATCAATGACAAGTCAACAGAAGGATTACTTTAAAGATAATT
GCGTCACCCACTACATGTGTGACGGGGAGACTTTTTTTGCTCGGGAATCGTCGAGTCACTGAACGTGCCTCTCCTC
ATACGAGTTTATCTAAAGTGATTATTTTTTTTGGGGTGTTTGTTTTTGGATTGTCTTTTTTTGTTTATTTCGTGTGTTA
TGTAACATATGTAATTTCTATCTACTTGCACAATGAAATATATTCATAAAATAATCATT

B

GAGGGTCGTACGAATAATTCGTATCCAACGGAAATACCTGATACAATATACGCTCCATCAAATACCATCACATCGTAT
ATGCTTTTATAGTGTGAACACCTTTAACCCTAGTGGGCGGGAAATTTTCTACTTTAAATCTGGACCGCTCGTGCTAA
AGCACTCGCGATAAGGGGGGGCCACGCCGGTAATATTAAATTCGGCGTGGGCCCCCCCTTGTCGCAAAGACTTCG
TCTTTAAGTAAATTCCACGTCATTTTCCACTATCTATTAAAATGACCAAAATACCCCTGCCTCCATGCCTCCACGCCG
GTTATAAGATAGAGTTTGAGGCAACCCCTCGGAGTCACAACAACTCCCAAAATGCCTTCTGCTAGTAAGAACTTCA
GACTCCAATCTAAATATGTTTTCCTTACCTATCCCAAGTGCTCATCTCAAAGAGATGATTTATTCCAGTTTCTCTGGG
AGAAACTCACACCTTTTCTTATTTTCTTCCTTGGTGTTGCTTCTGAGCTTCATCAAGATGGCACTACCCACTATCATG
CTCTTCTCCAGCTTGATAAAAAAACCTTGTATTAGGGATCCTTCTTTTTTCGATTTTGAAGGAAATCACCCTAATATCC
AGCCAGCTAGAAACTCTAAACAAGTCCTTGATTACATATCAAAGGACGGAGATATTAAAACCAGAGGAGATTTCC
GAGATCATAAGGTTTCTCCTCGCAAATCTGACGCACGATGGAGAACTATTATCCAGACTGCAACGTCTAAGGAGGA
ATATCTTGACATGATCAAGGAAGAATTCCCTCATGAATGGGCAACAAAGCTTCAATGGCTGGAATATTCAGCCAAC
AAATTATTCCCTCCACAACCTGAACCGTATGTGTCGCCCTTCACAGAATCAGATCTTCGCTGCCACGAAGATCTACA
CTCCTGGAGGGAAACCCATCTATACCATGTAAGCATAGACGCTTATACTTACATACATCCTGTCTCATACCAACAAGC
TCAATCTGACCTTGAATGGATGGCCGATTTAACAAGGACAATGGAAGGAATGGAATCCGACACCCCAGCCTCTAC
ATCTGCGGACCAACTCGTACCGGAAAGACCACCTGGGCTAGAAGTCTCGGACGACACAACTATTGGAACGGTAC
CATCGATTTCACCAACTACGATGAACACGCCACCTATAATATCATCGACGACATCCCCTTCAAGTTCGTCCCATTGTG
GAAGCAATTAATAGGTTGCCAGTCTGATTTCACTGTCAACCCTAAATATGGAAAAAAGAAGAAAATAAAAGGTGG
GATCCCTTCTATAATTCTTTGCAATCCTGACGAGGACTGGATGTTATCAATGACAAGTCAACAGAAGGATTACTTTA
AAGATAATTGCGTCACCCACTACATGTGTGACGGGGAGACTTTTTTTGCTCGGGAATCGTCGAGTCACTGAGGCA
ACGTGCCTCTCCTCATACGAGTTTATCTAAAGTGATTATTTTTTTTGGGGTGTTTGTTTTTGGATTGTCTTTTTTTGTT
TATTTCGTGTGTTATGTAACATATGTAATTTCTATCTACTTGCACAATGAAATATATTCATAAAATAATCATTTTAT

Supplemental Figure 1
Reengineering of the BeYDV Rep coding sequence used in the study.
(**A**) Reverse complement view of the LIR-Rep/RepA-SIR sequence isolated from pLSLR.
(**B**) Reverse complement view of the LIR-Rep/RepA-SIR sequence in the *de novo*-engineered replicon used in this study. Upper red font sequences: LIR; bottom red font sequences: SIR; purple sequences: Rep/RepA; green font: upstream ORF sequence (uORF); the light blue sequence TCCCAAA was inserted by cloning to interrupt uORF and add the Kozak preference sequence.

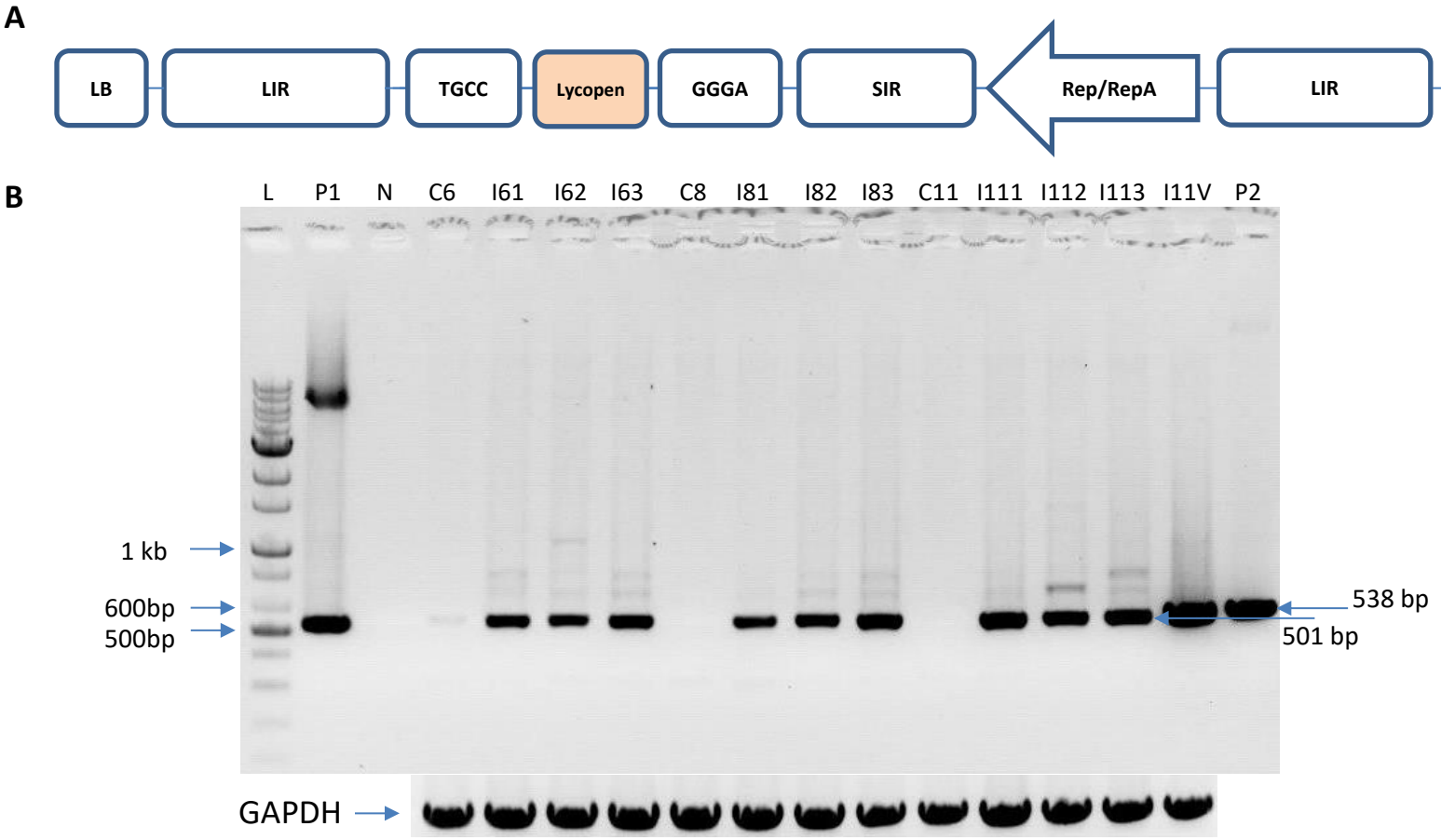

Supplemental Figure 2.
The *de novo*-engineered geminiviral amplicon (named pLSL.R. Ly) and its replication in tomato.
(**A**) Map of pLSL.R.Ly. The DNA amplicon is defined by its boundary sequences (long intergenic region, LIR) and a terminated sequence (short intergenic region, SIR). The replication-associated protein (Rep/RepA) is expressed from the LIR promoter sequence. All of the expression cassettes of HDR tools were cloned into the vector by replacing the red marker (Lycopene) using a pair of type IIS restriction enzymes (BpiI, flanking ends are TGCC and GGGA). Left (LB) and right (RB) denote the borders of a T-DNA.
(**B**) Circularized DNA detection in tomato leaves infiltrated with pLSL.R. Ly compared to those infiltrated with pLSLR. Agrobacteria containing the plasmids were infiltrated into tomato leaves (Hongkwang cultivar), and infiltrated leaves were collected at 6, 8 and 11 dpi and used for the detection of circularized DNAs. N: water; P1: positive control for pLSL.R. Ly; positive control for P2: pLSLR; Cx: Control samples collected at x dpi; Ixy: infiltrated sample number y collected at x dpi; I11 V: sample collected from leaves infiltrated with pLSLR at 11 dpi. PCR products obtained using primers specific to GAPDH were used as loading controls.

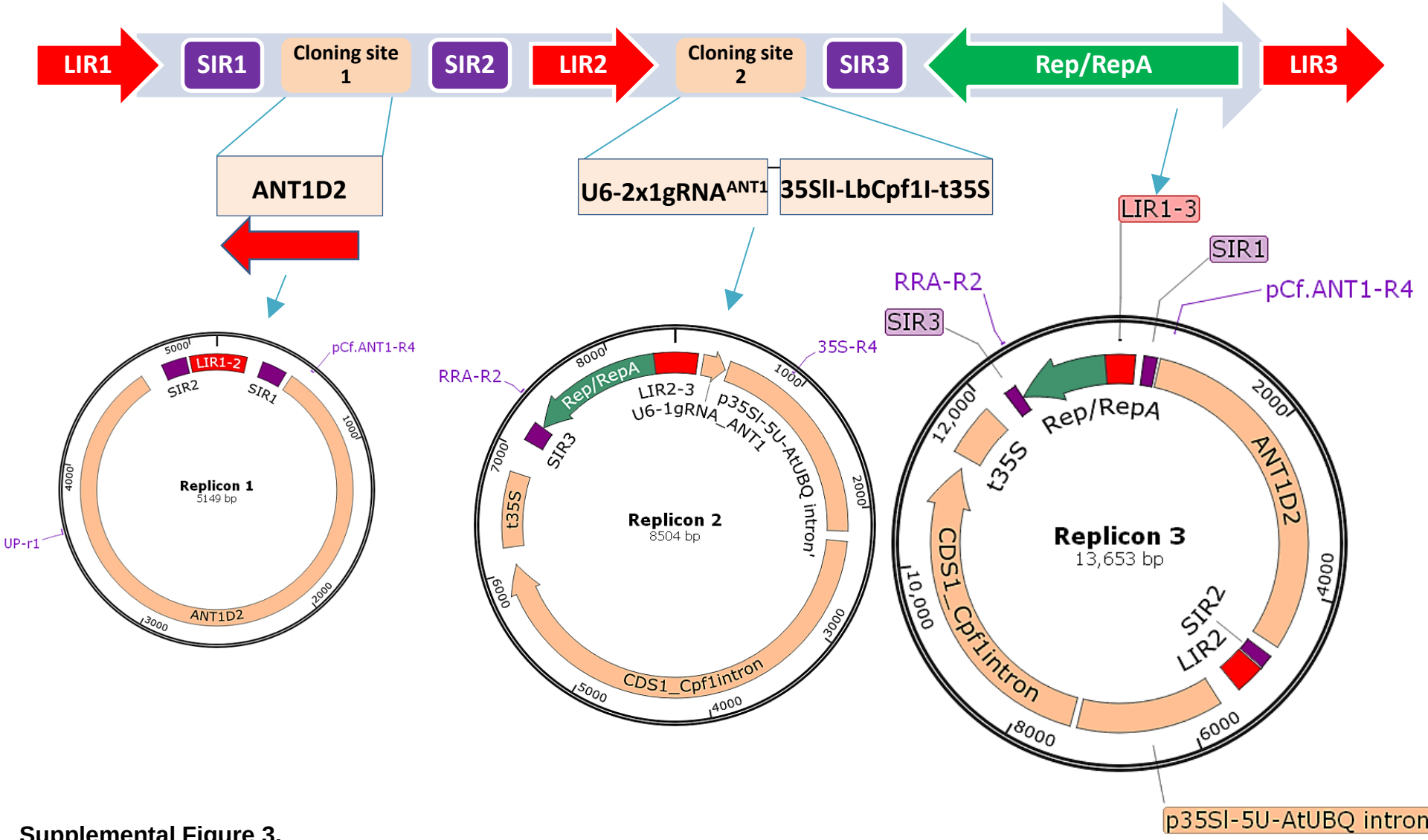

Supplemental Figure 3.
Schematic representation of the system and the released forms of the MR01 multiple replicon system.
Upper panel: The design for the general construction of multiple replicon complexes included three LIR and three SIR sequences. Middle panel: Representative arrangement of the MR01 tool. The donor template was cloned in one replicon, and the other components for inducing DSBs were located the other replicon. Bottom panel: Three replicons would be formed from the MR01. Primer pairs for detecting circularized replicon 1 (Upr1/pCf. ANT1-R4), replicon 2 (RRA-R2/35S-R4), and replicon 3 (RRA-R2/pCf. ANT1-R4) are indicated in the map of each replicon.

HDR GE0 plant hardening in vermiculite pot

HDR GE0 plant in greenhouse conditions

Flowers of HDR GE0 compared to wildtype plant

Fruits of HDR plant event C1.4

Fruit slices of HDR plant Fruit of HDR GE0 vs. wildtype plant

Supplemental Figure 4
Morphological appearance of GE0 plants.

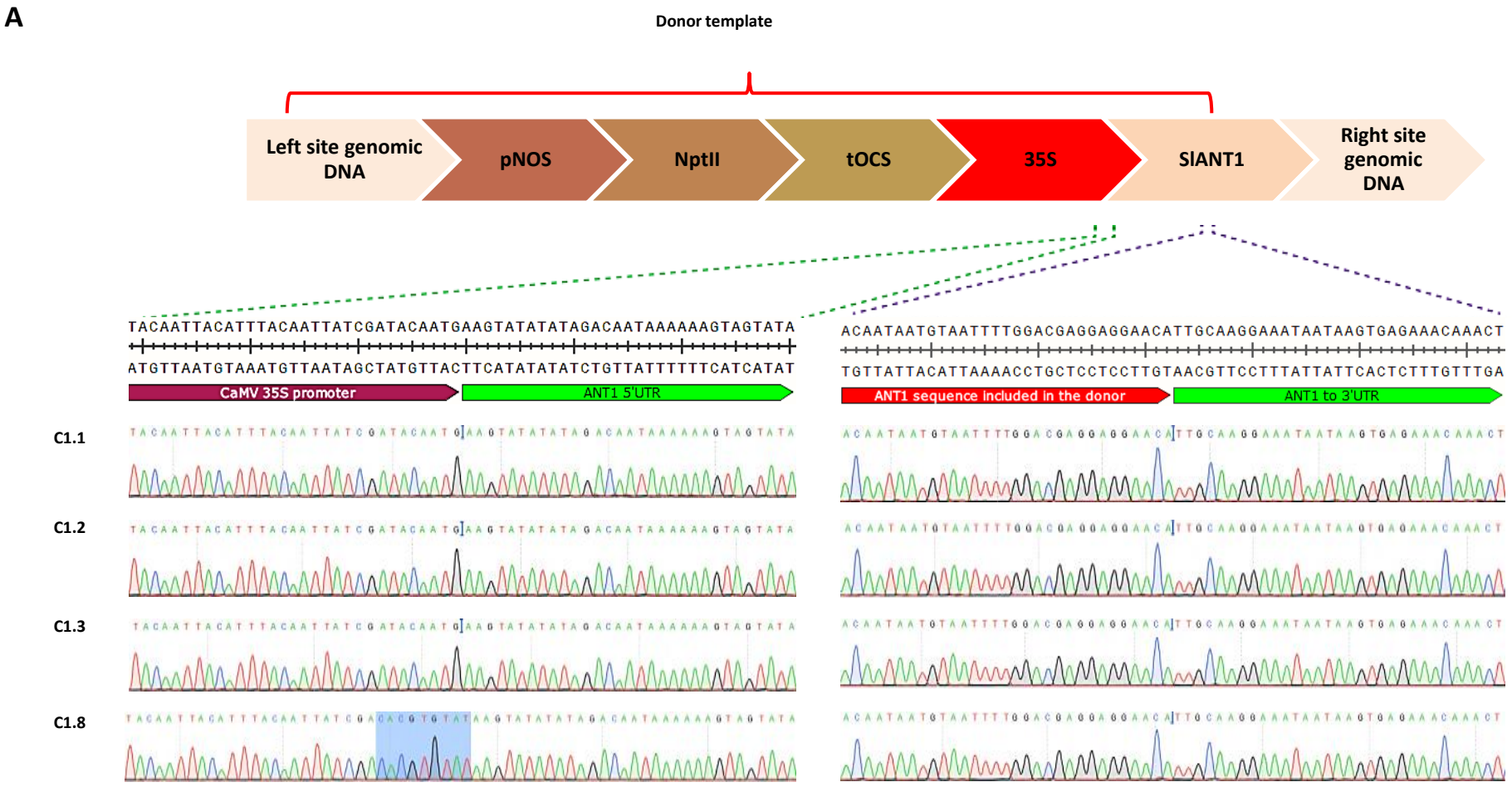

Supplemental Figure 5
Sanger sequencing data to confirm donor exchanges.
(**A**) Right junction.

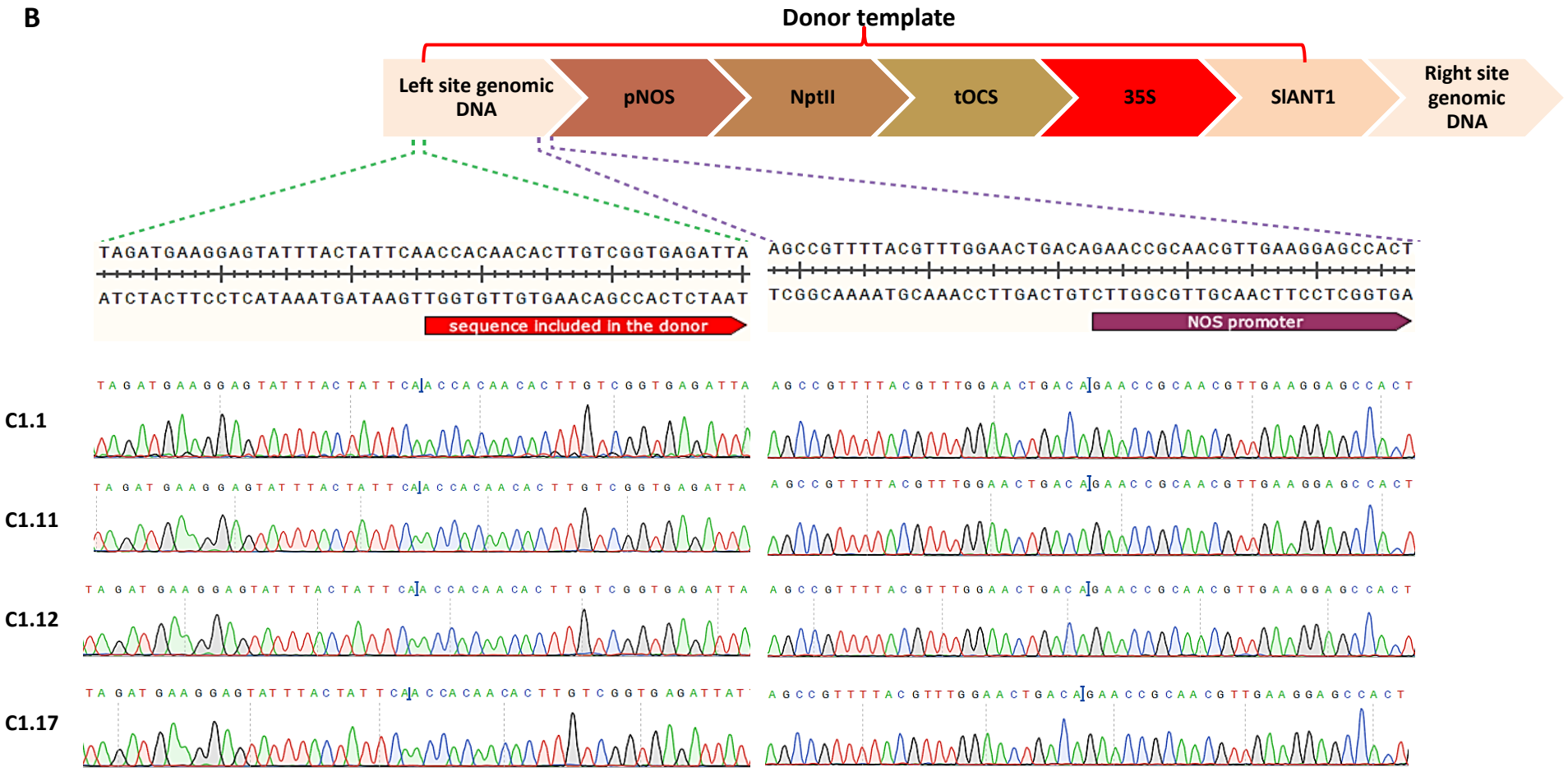

Supplemental Figure 5 (Continued)
Sanger sequencing data to confirm donor exchanges.
(**B**) Left junction. C1.1, C1.2, C1.3, C1.8, C1.11, C1.12, and C1.17: Independent LbCpf1-based HDR GE0 events

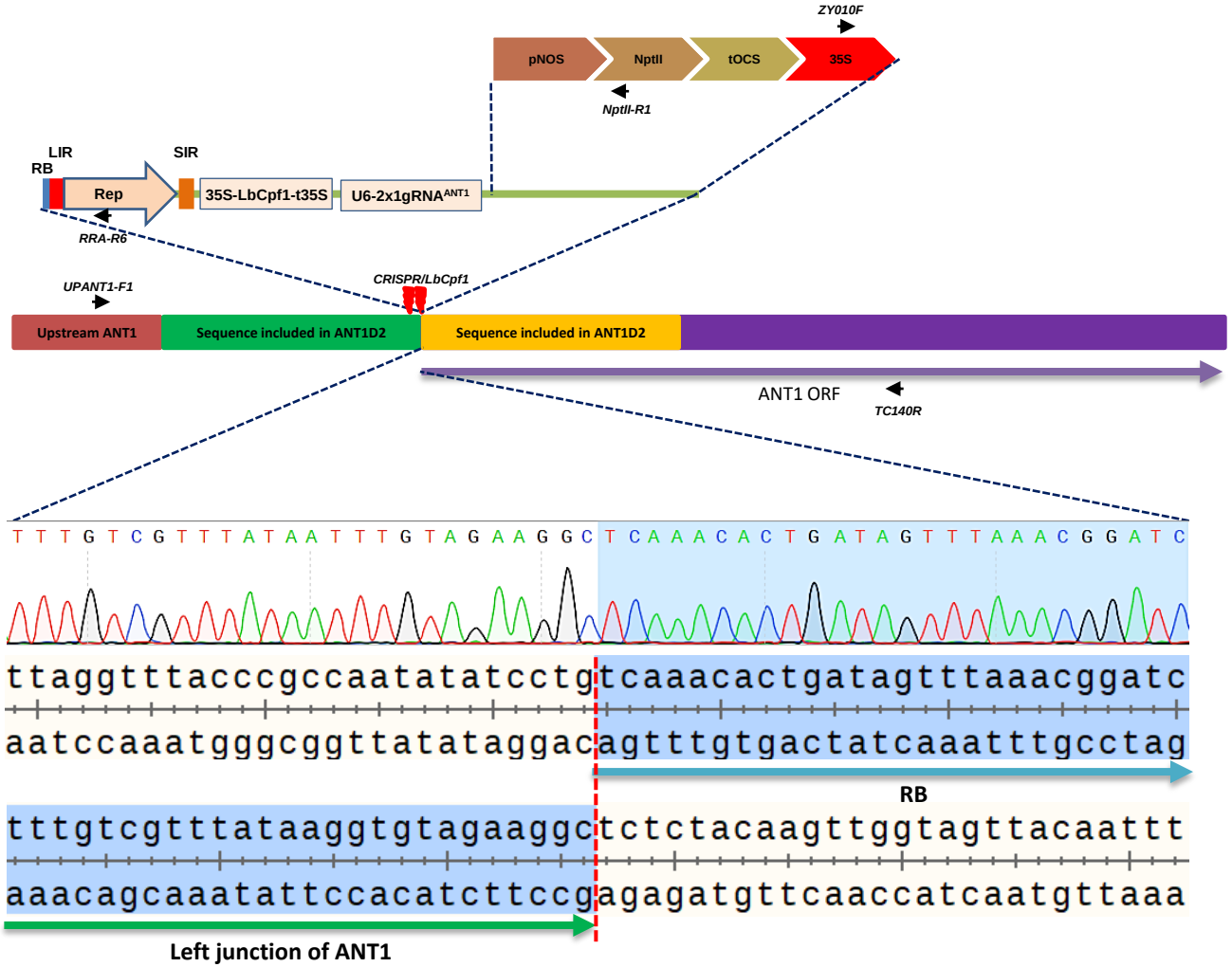

Supplemental Figure 6.

Error-prone repair combining HDR and NHEJ in event #C1.3.

The right junctions (amplified by ZY010F/TC140R) of the events were confirmed to be perfectly adapted to HDR repair (Supplemental Figure 5A), but the left junction could not be amplified (using the UPANT1-F1/NptII-R1 primer pair, Figure 1A). Sequencing of the left junction region showed a ligation event between the RB of the T-DNA and the 3' break in the upstream ANT1 promoter sequence via NHEJ. Red dotted line: ligation boundary.

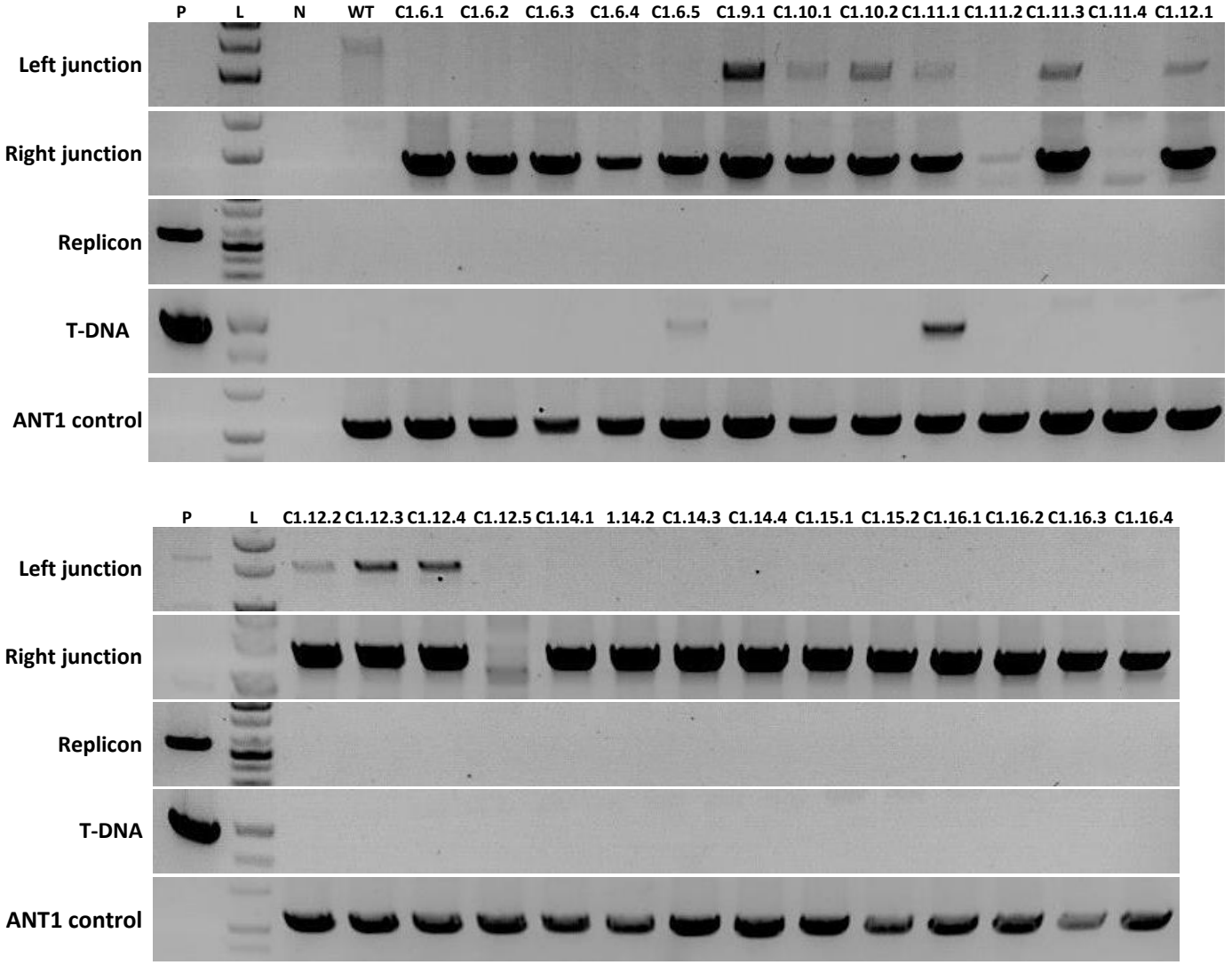

Supplemental Figure 7.
PCR analyses of GE1 plants obtained from GE0 LbCpf1-based HR events.
P: pHR01 plasmid isolated from Agrobacteria; L: 1 kb ladder; N: water control; WT: wild-type Hongkwang; C1.6.1-C1.6.5: GE1 offspring of event C1.6.; C1.9.1: GE1 offspring of event C1.9; C1.10.1 and C1.10.2: GE1 offspring of event C1.10; C1.11.1-C1.11.4: GE1 offspring of event C1.11; C1.12.1-C1.12.5: GE1 offspring of event C1.12; C1.14.1-C1.14.4: GE1 offspring of event C1.14; C1.15.1 and C1.15.2: GE1 offspring of event C1.15; C1.16.1-C1.16.4: GE1 offspring of event C1.16.

Heterozygous HDR GE1 plant (htHDR)

Homozygous HDR GE1 plant (hmHDR)

Phenotypes of GE2 plants compared to WT. GE2 offspring (left) of hmHDR GE1 plant back-crossed with WT (middle) resulted in all htHDR BC1F1 plants

hmHDR

WT

htHDR

Supplemental Figure 8
Morphological appearance of GE1 plants

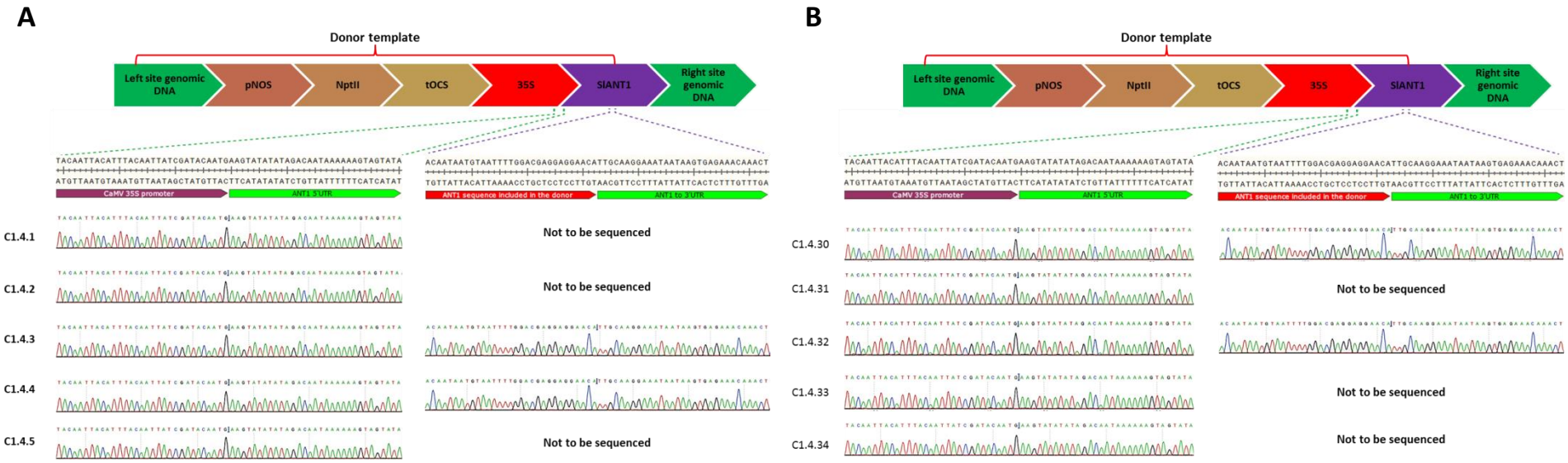

Supplemental Figure 9

Analyses of left and right junction sequences of GE1 plants.

Sanger sequencing data to confirm donor exchanges for the right (**A**) and left (**B**) junctions of the GE1 plants are presented

A

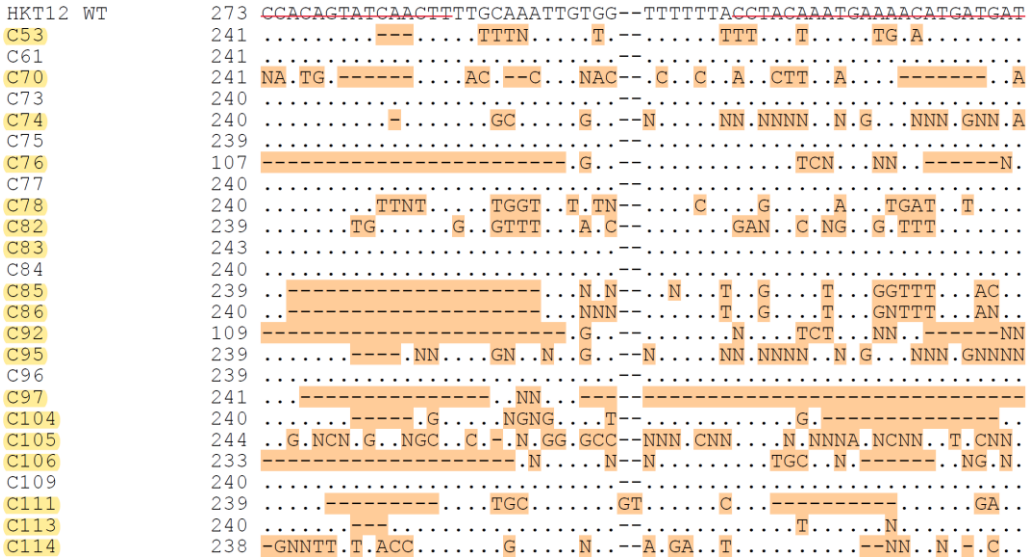

B

Supplemental Figure 10.
Analyses of indel mutations in HKT12 events.
(**A**) Alignment of raw sequences obtained from Sanger sequencing. 18/25 events (highlighted in yellow) showed strong double peaks indicating single/biallelic mutations. Six out of 25 events showed clear biallelic mutations. C77 showed weak (30%) double peaks. C83 and C105 showed large truncations. (**B**) Decomposed sequence of event #C53 obtained with ICE Synthego software.

Supplemental Figure 11.
Morphology of the heterozygous HKT12 D217 event in a mature stage
A plant resulting from the HKT12 D217 event (right) shows a normal morphology and fruit setting compared to the parental plant (left). Scale bars = 2 cm.

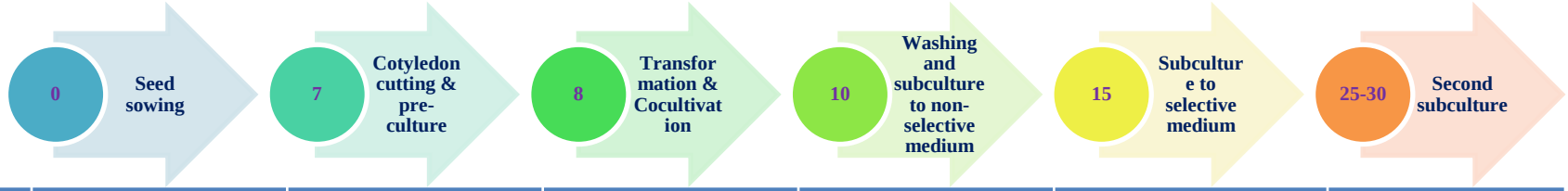

Stage	Germination	Pre-culture, calli induction	Co-cultivation, calli induction	Non-selection, calli induction	Selection, calli induction and shoot regeneration	Selection, shoot formation and elongation
Medium	MSO	PREMC,	ABM-MS	NSEL	SEL5	SEL5R
Temperature (°C)	25±2	25±1	25±1	31±1	28±1 for 5 days and then 25±2	25±2
Photoperiod	2 days-dark and then 16L/8D	1 day dark	2 days -dark	5 days-dark	5 days-8L/16D	16L/8D
Data collection	-	-	Sampling at 0dpt	Sampling at 3dpt and 6dpt	Sampling at 9dpt, Purple spot counting at 21 dpt	True shoot record

Supplemental Figure 12.
Timeline and contents of the *Agro*-mediated transformation protocol used in this work.
The step-by-step protocol is presented with each number in the circles indicating the number of days after seed sowing (upper panel), and the treatments used in each step are shown in the lower panel.

Supplemental Table 1. The increase in HDR by multiple replicon systems

No	Construct	Mean of HDR efficiency (%)*	Standard error of the mean (SEM) (%)	Fold change compared to pHR01	Fold change compared to pMR1	Donor template peak at 3 day post-transformation
1	pHR01	9.81[a]	0.48	1.00	1.44	1.00
2	MR01	6.82[c]	0.99	0.69	1.00	0.68
3	MR02	**12.79[b]**	0.37	**1.30**	**1.88**	**1.15**
4	MR03	12.26[ab]	1.39	1.25	1.80	1.56
5	MR04	8.33[c]	0.73	0.85	1.22	1.67

**Value with the same alphabet letter is not significantly different (t-test, n=4, p<0.05)*

Supplemental Table 2. Primers for detecting circularized replicons released by MR01 and pHR01

No.	Product	Primer name	Sequence (5’-3’)	Product length (bp)
1	Replicon 1 (MR01)	ANT1D2-cF1	CCAAATTTCCCAATGTACCTATCC	1980
2		pCf.ANT1-R4	ACCTCAACGACGCAAGTATT	
3	Replicon 2 (MR01)	RRA-R2	CATCCAGTCCTCGTCAGGATTGC	2063
4		35S-R4	CCTTCGAACTTCCTTCCTAGAT	
5	Replicon 3 (MR01)	RRA-R2	CATCCAGTCCTCGTCAGGATTGC	1725
6		pCf.ANT1-R4	ACCTCAACGACGCAAGTATT	
7	pHR01 Replicon	RRA-R2	CATCCAGTCCTCGTCAGGATTGC	1468
8		pCf.ANT1-R4	ACCTCAACGACGCAAGTATT	

Supplemental Table 3. Primers for LbCpf1-based HR event analyses

No.	Product	Primer name	Sequence (5'-3')	Product length (bp)
1	Left junction	UPANT1-F1	TGCGATGATCTACGGTAACAAA	1485
2		NPTII-R1	GCGTGCAATCCATCTTGTTC	
3	Right junction	ZY010F	ACGTAAGGGATGACGCACA	1380
4		TC140R	TACCACCGGTCCATTCCCTA	
5	ANT1 control	TC140F	GGAAAATGGCATCTTGTTCCC	1056
6		TC140R	TACCACCGGTCCATTCCCTA	
7	Replicon	GR-F1	TTGAGATGAGCACTTGGGATAG	557
8		pCf.ANT1-R4	ACCTCAACGACGCAAGTATT	
9	T-DNA	RB-qF2	CTCTTAGGTTTACCCGCCAATA	961
10		RRA-R6	GTTCAGGTTGTGGAGGGAATAA	
11	RB-ANT1D2 integration at the left junction of ANT1	UPANT1-F1	TGCGATGATCTACGGTAACAAA	2042
12		RRA-R6	GTTCAGGTTGTGGAGGGAATAA	

Supplemental Table 4. Primers for SpCas9-based HR event analyses

No.	Product	Primer name	Sequence (5’-3’)	Product length (bp)
1	Left junction	UPANT1-F1	TGCGATGATCTACGGTAACAAA	1485
2		NPTII-R1	GCGTGCAATCCATCTTGTTC	
3	Right junction	ZY010F	ACGTAAGGGATGACGCACA	1380
4		TC140R	TACCACCGGTCCATTCCCTA	
5	ANT1 control	TC140F	GGAAAATGGCATCTTGTTCCC	1056
6		TC140R	TACCACCGGTCCATTCCCTA	
7	Replicon	GR-F1	TTGAGATGAGCACTTGGGATAG	1198
8		35S-R3	CGTCAGTGGAGATGTCACATCA	

Supplemental Table 5. Phenotypic segregation of self-pollinated offspring resulting from LbCpf1-based HDR events.

No.	GE0 event	Total GE1 plants	Dark purple plant	hmHDR (%)*	Light purple plants	htHDR (%)**	WT-like	WT (%)
1	C1.4	113	30	26.5	37	32.7	46	40.7
2	C1.6	6	4	66.7	1	16.7	1	16.7
3	C1.9	1	1	100.0	0	0.0	0	0.0
4	C1.10	2	2	100.0	0	0.0	0	0.0
5	C1.11	10	5	50.0	4	40.0	1	10.0
6	C1.12	7	3	42.9	1	14.3	3	42.9
7	C1.14	4	4	100.0	0	0.0	0	0.0
8	C1.15	4	1	25.0	0	0.0	3	75.0
9	C1.16	7	3	42.9	2	28.6	2	28.6
Sum		154	53	34.4	45	29.2	56	36.4

*Dark purple or homozygous-like HDR plants
**Light purple or heterozygous-like HDR plants

Supplemental Table 6. Summary of the SlHKT1;2 HDR experiment

Total number of seeds (at 70% germination rate)	Total cotyledon fragment	Total analyzed events	Total Potential HDR events	Total true HDR events	HDR efficiency
460	640*	150	09	01	0.66%**

*Can be done in only one transformation.
**HKT1;2 gene donor template contains neither antibiotic selection marker nor ANT1 color marker.

Supplemental Table 7. Indel mutation rates among *HKT12* samples decomposed by ICE Synthego software

No.	Event	ICE score	KO-Score	ICE d	R Squared	Mean Discord Before	Mean Discord After
1	C105	N/A*	N/A	N/A	N/A	N/A	N/A
2	C78	58	56	61	0.95	0.072	0.504
3	C95	97	48	91	0.97	0.063	0.719
4	C74	49	49	41	0.98	0.07	0.556
5	C104	78	40	97	0.78	0.068	0.719
6	C77	14	9	14	1	0.084	0.226
7	C86	49	49	50	0.93	0.08	0.53
8	C73	1	1	1	1	0.077	0.18
9	C96	1	1	1	1	0.072	0.163
10	C70	N/A	N/A	N/A	N/A	N/A	N/A
11	C75	3	2	3	1	0.065	0.253
12	C97	47	44	90	0.48	0.075	0.7
13	C76	6	6	95	0.06	0.347	0.706
14	C114	90	46	92	0.9	0.08	0.708
15	C85	48	48	48	0.93	0.067	0.491
16	C106	48	46	95	0.48	0.076	0.708
17	C82	50	2	46	0.96	0.074	0.439
18	C84	2	2	2	1	0.074	0.168
19	C111	84	37	92	0.84	0.07	0.704
20	C83	14	11	13	0.97	0.075	0.219
21	C109	3	1	3	1	0.075	0.176
22	C61	0	0	0	1	0.075	0.136
23	C53	58	14	50	0.96	0.081	0.436

* Highly variable sequence at the targeted site might be due to large deletion